

## AT 2024ahzi: A Type IIP Supernova Discovered by the LSST Commissioning Camera

KAYLEE DE SOTO,<sup>1</sup> V. ASHLEY VILLAR,<sup>1,2</sup> JARED A. GOLDBERG,<sup>3,4</sup> ANYA NUGENT,<sup>1</sup> YIZE DONG (董一泽),<sup>1,2</sup>  
RYAN J. FOLEY,<sup>5</sup> TOBIAS GÉRON,<sup>6</sup> LUCA IZZO,<sup>7,8</sup> C. TANNER MURPHEY,<sup>9,10,11</sup> KATIE AUCHETTL,<sup>5,12</sup>  
DAVID A. COULTER,<sup>13,14</sup> THOMAS DE BOER,<sup>15</sup> KENNETH C. CHAMBERS,<sup>15</sup> DIEGO A. FARIAS,<sup>7</sup> CHRISTA GALL,<sup>7</sup> HUA GAO,<sup>15</sup>  
JENS HJORTH,<sup>7</sup> WILLEM B. HOOGEN DAM,<sup>15</sup> DAVID O. JONES,<sup>16</sup> GAURI NAIR,<sup>9</sup> GAUTHAM NARAYAN,<sup>9,10,17</sup> ARMIN REST,<sup>13,14</sup>  
KISHORE C. PATRA,<sup>5</sup> HAILLE M. L. PERKINS,<sup>9</sup> MARGARET E. VERRICO,<sup>9</sup> QINAN WANG,<sup>18</sup> AMANDA R. WASSERMAN,<sup>9</sup> AND  
YOSSEF ZENATI<sup>19,13</sup>

<sup>1</sup>Center for Astrophysics | Harvard & Smithsonian, 60 Garden Street, Cambridge, MA 02138-1516, USA

<sup>2</sup>The NSF AI Institute for Artificial Intelligence and Fundamental Interactions

<sup>3</sup>Department of Physics and Astronomy, Michigan State University, East Lansing, MI 48824, USA

<sup>4</sup>Center for Computational Astrophysics, Flatiron Institute, 162 5th Avenue, New York, NY 10010, USA

<sup>5</sup>Department of Astronomy and Astrophysics, University of California, Santa Cruz, CA 95064, USA

<sup>6</sup>David A. Dunlap Institute of Astronomy & Astrophysics University of Toronto, Toronto, ON, M5S 3H4, Canada

<sup>7</sup>DARK, Niels Bohr Institute, University of Copenhagen, Jagtvej 128, 2200 Copenhagen, Denmark

<sup>8</sup>INAF, Osservatorio Astronomico di Capodimonte, salita Moiariello 16, I-80131, Naples, Italy

<sup>9</sup>Department of Astronomy, University of Illinois at Urbana-Champaign, 1002 W. Green St., IL 61801, USA

<sup>10</sup>Center for Astrophysical Surveys, National Center for Supercomputing Applications, Urbana, IL, 61801, USA

<sup>11</sup>Illinois Center for Advanced Studies of the Universe, Urbana, IL 61801

<sup>12</sup>OzGrav, School of Physics, The University of Melbourne, VIC 3010, Australia

<sup>13</sup>William H. Miller III Department of Physics & Astronomy, Johns Hopkins University, 3400 N Charles St, Baltimore, MD 21218, USA

<sup>14</sup>Space Telescope Science Institute, Baltimore, MD 21218, USA

<sup>15</sup>Institute for Astronomy, University of Hawai'i, 2680 Woodlawn Drive, Honolulu, HI 96822, USA

<sup>16</sup>Institute for Astronomy, University of Hawai'i, 640 N. Aohoku Pl., Hilo, HI 96720, USA

<sup>17</sup>NSF-Simons SkAI Institute, 875 N. Michigan Ave., Chicago, IL 60611, USA

<sup>18</sup>Department of Physics and Kavli Institute for Astrophysics and Space Research, Massachusetts Institute of Technology, 77 Massachusetts Avenue, Cambridge, MA 02139, USA

<sup>19</sup>Astrophysics Research Center of the Open University (ARCO), Department of Natural Sciences, Ra'anana 4353701, Israel

### ABSTRACT

As part of its commissioning, the Vera C. Rubin Observatory observed several fields repeatedly for a month with ComCam, an instrument that uses the same hardware as the LSST camera but covers a smaller field of view. We photometrically classify AT 2024ahzi, a transient discovered by ComCam, as a Type IIP supernova (SN IIP) using both ComCam and DECam photometry. We find that the duration, luminosity, and color of AT 2024ahzi's photometric plateau are all consistent with those from a large sample of SNe II. By comparing its multi-band light curves to SN II models and analytic relations, we place constraints on the SN progenitor, explosion dynamics, and circumstellar environment. We argue that the progenitor has an extended density profile indistinguishable from a slowly accelerating CSM. We discuss how a similar workflow can identify and characterize future Rubin SNe II.

### 1. INTRODUCTION

Core-collapse supernovae (CCSNe) are the endpoints of massive stars and are important drivers of the chemical evolution of the Cosmos (S. J. Smartt et al. 2009; A. Jerkstrand et al. 2025). The most common subclass of CCSNe, SNe IIP, are characterized by months-long plateaus in their light curves from the cooling and

recombination of hydrogen-rich envelopes (A. V. Filippenko 1997; S. J. Smartt et al. 2009; W. Li et al. 2011; N. Smith et al. 2011; A. Gal-Yam 2017). SNe IIP are traditionally contrasted with SNe IIL, which have a linear brightness decline and tend to be brighter than SNe IIP (R. Barbon et al. 1979; F. Patat et al. 1994). Recent studies suggest that SNe IIP and SNe IIL form a continuum rather than two distinct subclasses (J. P. Anderson et al. 2014; E. E. E. Gall et al. 2015; N. E. Sanders et al. 2015; L. Galbany et al. 2016; S. Valenti et al. 2016;

J. P. Anderson et al. 2024) The brightness, duration, and multiband color of SN IIP plateaus provide insight into their underlying explosion dynamics and progenitor properties (D. V. Popov 1993; A. Chieffi et al. 2003; M. Hamuy 2003; T. R. Young 2004; O. Pejcha & J. L. Prieto 2015; J. A. Goldberg et al. 2019; D. Hiramatsu et al. 2021; L. Martinez et al. 2022a).

There is increasing evidence for dense circumstellar matter (CSM) surrounding CCSNe, formed from mass lost via stellar winds, stellar outbursts, or binary envelope stripping (O. Yaron et al. 2017; A. Kozyreva et al. 2022; I. Irani et al. 2024; W. V. Jacobson-Galán et al. 2024; K. R. Hinds et al. 2025; T. Nagao et al. 2025). The supernova ejecta’s interaction with the CSM manifests as a bright blue continuum with or without narrow Lorentzian emission lines, as photons scatter off free electrons before leaving the CSM (N. N. Chugai 2001). The prevalence of CSM around SNe II, and whether it explains the continuum between SNe IIP and SNe IIL, both remain open questions (V. Morozova et al. 2017, 2018; K. A. Bostroem et al. 2019; D. Hiramatsu et al. 2021). Early high-ionization flash features and rapid optical rise timescales have been found in >36% (D. Khazov et al. 2016; R. J. Bruch et al. 2021; R. J. Bruch et al. 2023) and > 90% of typical SNe II (F. Förster et al. 2018), respectively, both indicative of a confined CSM (S. W. Falk & W. D. Arnett 1977; A. P. Nagy & J. Vinkó 2016; Hillier, Desmond John & Dessart, Luc 2019; R. J. Bruch et al. 2021).

There have been  $\sim 4,000$  detected and spectroscopically classified SNe II so far, with most detected by the Zwicky Transient Facility (ZTF; F. J. Masci et al. 2018; D. A. Perley et al. 2020) and the Asteroid Terrestrial-impact Last Alert System (ATLAS; J. L. Tonry et al. 2018)<sup>20</sup>. Both observe the night sky every two days in *gr*- and cyan/orange bands, respectively, with ZTF limited to the northern sky. While two bands are often sufficient for classification, they cannot robustly constrain both blackbody temperature and photospheric radius. Along the hydrogen-recombination plateau (at 6000 K), the *g*- and *r*-bands straddle the continuum peak, so extracted blackbody temperatures are more confident. At early phases, however, blackbody temperatures exceed  $\sim 10,000$  K, and both wavelengths lie on the Rayleigh-Jeans tail. This, along with biases from optical emission lines and UV iron-element line blanketing, means that early-phase blackbody temperatures are overestimated without near-UV observations. Previous works find bi-

ases of  $\sim 10$ -50% (L. Dessart & D. J. Hillier 2005; S. Valenti et al. 2016; T. Faran et al. 2017).

The Vera C. Rubin Observatory Legacy Survey of Space and Time (LSST) will detect SNe at a limiting flux  $\sim 40$  times fainter than ZTF (LSST Science Collaboration et al. 2009). It is expected to find  $\sim 300,000$  CCSNe annually (R. Kessler et al. 2019), at a median redshift of  $\sim 0.2$ . This two-order-of-magnitude increase in sample size will allow us to characterize the diversity in photometric evolution among SNe IIP to high precision, especially at redshifts beyond 0.1. Establishing relations between progenitor properties and SN II photometry will allow for more certain conclusions regarding the perceived lack of  $> 18M_{\odot}$  SN II progenitors (dubbed the missing red supergiant problem; S. J. Smartt et al. 2009; S. J. Smartt 2015; C. S. Kochanek 2020). While this discrepancy between RSG and SN II progenitor mass limits can be attributed to failed SNe (C. S. Kochanek et al. 2008; S. M. Adams et al. 2017; J. M. M. Neustadt et al. 2021), it can also be attributed to observational biases (J. J. Walmswell & J. J. Eldridge 2012; B. Davies & E. R. Beasor 2017; C. D. Kilpatrick et al. 2023; E. R. Beasor et al. 2024; N. L. Strotjohann et al. 2024) or small-number statistics (B. Davies & E. R. Beasor 2020; S. Healy et al. 2024). Large photometric SN II samples could better populate the high-mass progenitor tail by assuming a correlation between plateau properties and progenitor mass (D. Kasen & S. E. Woosley 2009; L. Dessart et al. 2010; J. A. Goldberg et al. 2019; B. L. Barker et al. 2022, 2023).

LSST will cycle between *ugrizy* filters. At typical expected redshifts, the *u*-band will probe the near-to-mid UV, which aligns with temperatures of shock breakout augmented by CSM (E. Waxman & B. Katz 2017; I. Irani et al. 2024). The near-IR bands will improve blackbody fits by avoiding iron-element line blanketing (L. Martinez et al. 2022b) and experiencing less extinction from dust.

As part of preparation for LSST, the Rubin commissioning camera (dubbed ComCam), conducted preliminary science observations from November 4, 2024 to December 10, 2024, collating all detections and forced photometry in the Data Preview 1 (DP1; Rubin Observatory Science Pipelines Developers 2025; NSF-DOE Vera C. Rubin Observatory 2025). These observations were taken in a handful of fields at a  $\sim 1$ -3 day cadence.

In this paper, we photometrically classify and analyze AT 2024ahzi, making it the first photometrically classified SN IIP after detection by the Rubin Observatory. We simultaneously observed AT 2024ahzi with the Dark Energy Camera (DECam), which captured its full plateau and increased classification confidence.

<sup>20</sup> [www.wis-tns.org](http://www.wis-tns.org)

In Section 2 we detail how we collated DECam photometry, prioritized SN candidates, and retrieved ComCam photometry for overlapping events. In Section 3, we associate AT 2024ahzi to a host galaxy and infer the host’s redshift, dust extinction, and star formation history. In Section 4, we model AT 2024ahzi’s joint ComCam-DECam photometry to characterize its evolution over time and estimate its circumstellar and progenitor properties. In Section 5, we show that AT 2024ahzi’s plateau properties are congruent with those from a large, low- $z$  SN IIP population. We summarize our findings in Section 6 and provide recommendations for future Rubin SN IIP identification.

## 2. OBJECT SELECTION AND DATA COLLATION

### 2.1. Transient Identification with DECam

The Young Supernova Experiment (YSE; D. O. Jones et al. 2021) collaboration used the Dark Energy Camera (DECam; B. Flaugher et al. 2015) mounted on the 4-m Victor M. Blanco Telescope at the Cerro Tololo Inter-American Observatory (CTIO) to observe the Euclid Deep Field South (EDFS) and Extended Chandra Deep Field South (ECDFS) fields (NOIRLab PropIDs 2024B-763968, 2024B-441839, and 2025A-388357). YSE observed the EDFs field 414 times in *griz* between November 26, 2024 and April 27, 2025, and the ECDFS field 366 times between August 22, 2024 and April 18, 2025. Data were initially processed by the NOIRLab Community Pipeline and then transferred to the Illinois Campus Cluster. The images were then processed using the *Photpipe* difference imaging and forced photometry pipelines (A. Rest & SuperMACHO 2004; A. Rest et al. 2014).

After performing standard data reductions on NOIRLab images (i.e., masking saturated pixels, correcting optical distortions, and basic photometry using DoPHOT; P. L. Schechter et al. 1993), *Photpipe* subtracts template images from science images using HOTPANTS (A. Becker 2015). Template images are selected to avoid including flux from the transients themselves; identification of AT 2024ahzi used templates from November 6, 2024. Possible transients are identified as coordinates with at least three  $3\sigma$  detections across multiple consecutive observing nights. YSE astronomers manually filter these candidates by examining the forced photometry and difference images.

AT 2024ahzi was first detected on December 19, 2024 in DECam’s *Euclid* Deep Field South (EDFS) field, identified by YSE astronomers on January 22, 2025, and reported to the *Transient Name Server* (TNS) on March 13, 2025 (C. T. Murphey et al. 2025). It is located at R.A. =  $03^{\text{h}}53^{\text{m}}20^{\text{s}}.41$ , Dec =  $-48^{\circ}45'01''.09$ .

### 2.2. Cross-matching with ComCam Objects

ComCam obtained *ugrizy* observations of seven fields from November 4, 2024 to December 10, 2024 (Rubin Observatory Project 2025) as part of LSST commissioning. Concurrent DECam observations overlap with the ComCam ECDFS and EDFs fields; we show the EDFs overlap in Figure 1. We only consider DECam candidates within this overlapping region that were observed at least once between July 27, 2024 and January 9, 2025, as a generous buffer around the ComCam observing window. These constraints yield 61 DECam candidates in ECDFS and 8 in EDFs.

We then query the DP1 *DiObject* catalog for all objects with difference-image detections that coincide with our remaining DECam candidates. We find matches for 7 events in ECDFS and 2 events in EDFs. Among these, AT 2024ahzi (designated by Rubin as LSST-DP1-DO-592914119179370575) shows clear SN IIP-like evolution in the joint ComCam-DECam photometry. The remaining events are analyzed in T. Murphey (in prep.).

### 2.3. Template Correction and Pre-processing

DP1 provides forced photometry extracted from ComCam difference images. However, the templates used for difference imaging are a coadded subset of the ComCam science images and contain the SN signal itself. We therefore use deep coadded DECam images from the Dark Energy Survey Data Release 2 (DES DR2, Dark Energy Survey Collaboration et al. 2016; T. M. C. Abbott et al. 2021) as templates for difference imaging. These DECam images were taken between 2013 and 2019, well before the SN explosion. The image subtraction and photometry extraction are performed using the SLIDE<sup>21</sup> package (Y. Dong et al. 2025), which is designed for LSST image subtraction using DECam templates and can run directly on the Rubin Science Platform. We only apply this template subtraction on *griz* ComCam images, since there are no appropriate *u*- and *y*-band DES templates to use.

Individual observations within the same night and with the same filter are combined using a weighted average. As the provided uncertainties are generally much smaller than the spread among same-night observations, we instead quantify each nightly flux uncertainty as the median absolute deviation of per-night fluxes in each filter.

We also use SLIDE and DES templates to re-subtract DECam images, rather than the *Photpipe* pipeline detailed above. We do this because DES’s images are

<sup>21</sup> <https://github.com/yizedong/SLIDE>

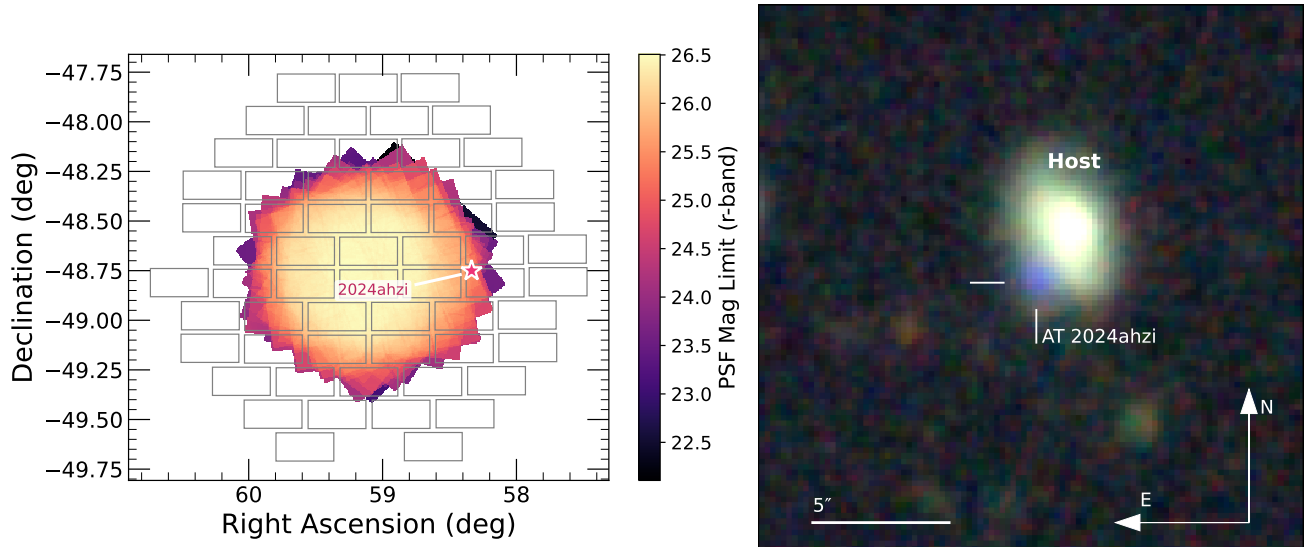


**Figure 1.** *Left:* ComCam exposure map showing the location of AT 2024ahzi and a single DECcam pointing overlaid. Grey rectangles represent single DECcam CCDs. *Right:* A ComCam *gri* color-composite image of the field surrounding AT 2024ahzi. The SN is circled and the crosshairs show the location of the host, which has a spectroscopic redshift  $z = 0.211 \pm 0.002$ .

**Table 1.** Subset of nightly co-added observations of AT 2024ahzi, uncorrected for Milky Way or host extinction. We include the first  $5\sigma$  detection preceded by the last two non-detections. All uncertainties are  $1\sigma$ . The full single-exposure and nightly co-added photometry are available as machine readable tables online.

MJD	Instrument	Filter	AB Mag	AB Mag Unc.	Flux ( $\mu\text{Jy}$ )	Flux Unc. ( $\mu\text{Jy}$ )
60641.110	ComCam	i	24.188 <sup>†</sup>	—	-0.307	0.153
60641.119	ComCam	r	25.888 <sup>†</sup>	—	-0.366	0.032
60647.135	ComCam	r	22.664	0.088	3.121	0.253
60649.257	DECcam	g	22.111	0.083	5.196	0.397
60649.258	DECcam	r	22.413	0.195	3.935	0.708
60649.259	DECcam	i	22.406	0.181	3.959	0.660
60652.170	DECcam	g	22.353	0.111	4.159	0.426
60652.171	DECcam	r	22.454	0.122	3.787	0.426
60652.172	DECcam	i	22.367	0.167	4.103	0.632
60653.233	ComCam	r	22.430	0.054	3.874	0.191
60653.234	ComCam	g	22.223	0.032	4.685	0.137
60653.240	ComCam	z	22.460	0.148	3.768	0.514

<sup>†</sup>  $5\text{-}\sigma$  non-detection upper limit

deeper than DECcam’s, resulting in less noisy subtractions for extremely faint observations. This only has a significant impact on the *g*-band observations, which are  $\text{SNR} < 3$  non-detections along the plateau; as we are working in flux space, we can still use these observations to constrain plateau properties.

Because DECcam and ComCam have similar filter profiles, we combine observations across the two instruments. DECcam’s *z* bandpass has a secondary bump

around 9700 angstroms that ComCam lacks. We argue, however, that since there is only one ComCam *z*-band observation, the filter mismatch has a minimal impact on downstream analysis. The resulting nightly co-added *griz*-band photometry after improved template subtraction is in Table 1. We highlight the improvement in difference-image ComCam photometry compared to the DP1 values in Figure 2. Improved continuity from ComCam to DECcam photometry with the corrected tem-

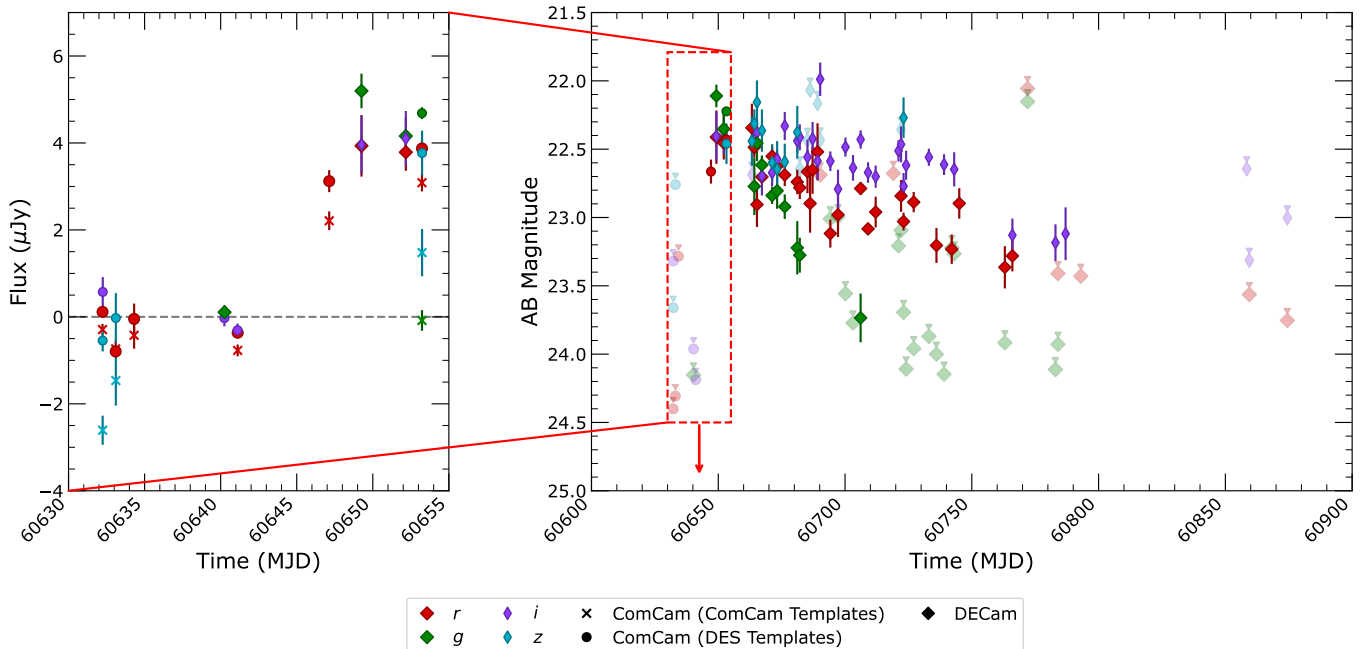


**Figure 2.** *Left:* Comparison of ComCam *griz*-band difference-image photometry of AT 2024ahzi as queried directly from RSP (i.e., using the ComCam templates; circles), versus corrected using robust DES templates (squares). The DECam difference-image photometry at early times is also included (triangles) to highlight the improved continuity between instruments when using the DES-subtracted ComCam photometry. *Right:* The combined AT 2024ahzi light curves in magnitude space. Translucent points represent 3-sigma upper limits of non-detections ( $\text{SNR} \leq 3$ ). For clarity, only the DES-subtracted ComCam photometry is shown.

plates is especially visible in the corrected *g*-band data. From MJD 60652 to MJD 60653, there is an  $8\sigma$  *g*-band jump between the DECam and ComCam observations using ComCam templates; with DES templates, the two observations agree within  $1\sigma$ .

AT 2024ahzi’s first detection is  $22.66 \pm 0.09$  mag, taken by ComCam at MJD 60647 in the *r*-band. To confirm that this is a real detection, we apply the DETECT pipeline (T. Géron 2024) to estimate the detection thresholds for the corresponding template and visit images. We find 50% and 80% detection thresholds of  $> 23.52$  mag and  $> 23.49$  mag, respectively. Our observation is brighter than these thresholds and, therefore, considered a true detection. We constrain AT 2024ahzi’s time of explosion between December 3, 2024 (MJD 60641) and December 9, 2024 (MJD 60647).

### 3. HOST GALAXY ANALYSIS

Because both redshift and dust extinction can significantly alter AT 2024ahzi’s photometry and therefore our downstream analysis, we first constrain these values through host galaxy association.

In Figure 1 AT 2024ahzi is coincident with WISEA J035320.41-484500.0, a face-on spiral galaxy located at R.A. =  $03^{\text{h}}53^{\text{m}}20^{\text{s}}.304$ , Dec =  $-48^{\circ}44'59''.28$ . We for-

mally associate the host galaxy of AT 2024ahzi to its host galaxy using Pröst<sup>22</sup>, a Bayesian transient association code (A. Gagliano et al. 2025). From the galaxy’s brightness distribution and the offset between SN and galaxy, Pröst confidently associates AT 2024ahzi to WISEA J035320.41-484500.0 with a chance coincidence probability of 0.002 (using the formula in J. S. Bloom et al. 2002). With a host-SN offset of  $2.107''$  and a host *g*-band half-light radius of  $2.111''$ , we retrieve a relative offset  $\approx 1$ , which is within the interquartile range of the SN II sample from (P. L. Kelly & R. P. Kirshner 2012). The host galaxy is recovered from the DECaLS DR9 catalog, with a photometric redshift of  $z_{\text{phot}} = 0.202 \pm 0.058$ .

The photometric redshift uncertainty corresponds to an uncertainty in distance modulus that is too large for downstream SN analysis. To extract a more precise redshift, we obtain a spectrum of the host using the Low Dispersion Survey Spectrograph (LDSS-3; K. Boutsia et al. 2016) on the Magellan Clay telescope (P.I. Gagliano). We observe the [OII] $\lambda$ 3727, H $\beta$ , [OIII] $\lambda$  $\lambda$ 4959, 5007, [NII] $\lambda$  $\lambda$ 6548, 6584, H $\alpha$ , and [SII] $\lambda$  $\lambda$

<sup>22</sup> <https://github.com/alexandergagliano/Prost>

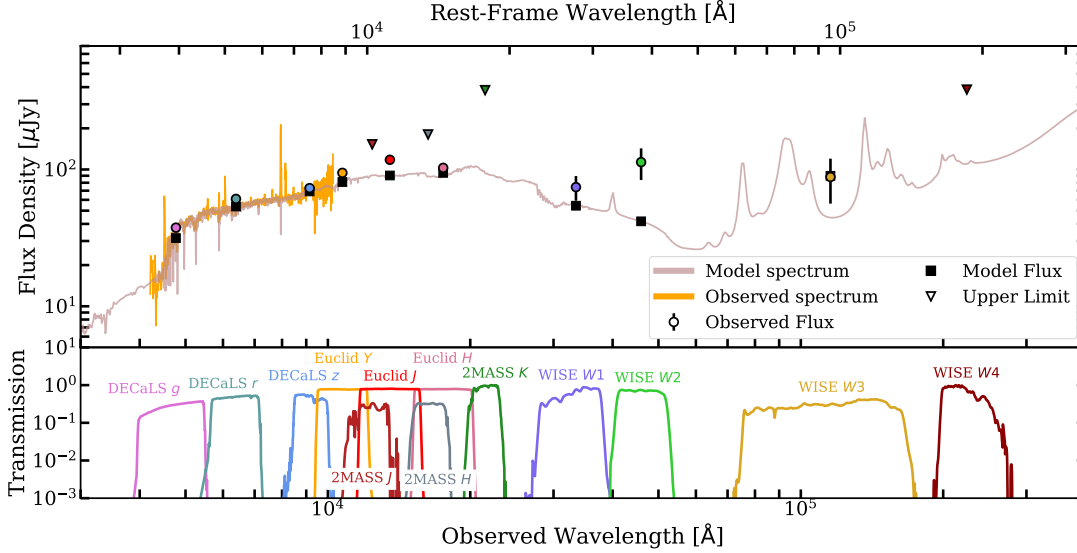


**Figure 3.** Observed photometry (colored circles) and spectrum (gold line) obtained of AT 2024ahzi’s host galaxy, compared to the *Prospector* model spectrum (purple line) and corresponding photometry (black squares). The model suggests that the host is actively star-forming, consistent with the blue observed color of the host in the composite image.

6717,6731 emission lines. Fitting these lines with a Gaussian distribution, we determine that the host lies at  $z = 0.211 \pm 0.002$ . This is statistically consistent with the photo- $z$  recovered by Pröst.

We use a customized version of *Blast* (D. O. Jones et al. 2024), which we call *FrankenBlast* (A. E. Nugent et al. 2025), to extract host-galaxy photometry. *FrankenBlast* collects images of the host galaxy from DECaLS DR9, the *Two Micron All-Sky Survey* (2MASS; M. F. Skrutskie et al. 2006), and the *Wide-field Infrared Survey Explorer* (WISE; E. L. Wright et al. 2010). For every archival image, *FrankenBlast* constructs elliptical apertures surrounding the host with the *Astropy photutils* package (L. Bradley et al. 2025). These apertures are optimized for each image independently. In the 2MASS *JHK* and WISE *W4* bands, where the host is not detected, we use the aperture size of a neighboring filter. This aperture optimization differs from the method used in D. O. Jones et al. (2024), which uses consistent, PSF-adjusted aperture sizes across all wavelengths. As a result, *FrankenBlast* extracted fluxes are less noisy, but potentially underestimated in the IR and UV.

To complement the photometry retrieved with *FrankenBlast*, we collect *YJH* photometry from *Euclid* (Euclid Collaboration et al. 2025a). *Euclid* photometry is retrieved from the *Euclid* Q1 MER final catalog (Euclid Collaboration et al. 2025b) using the *astroquery* package (A. Ginsburg et al. 2019). NIR fluxes are extracted from single Sersic model fitting, as measured with Source Extractor (E. Bertin & S. Arnouts 1996; M. Kümmel et al. 2022), and converted to AB magni-

Survey	Filter	AB Mag
DECaLS	<i>g</i>	$19.96 \pm 0.01$
DECaLS	<i>r</i>	$19.43 \pm 0.01$
DECaLS	<i>z</i>	$19.24 \pm 0.02$
2MASS	<i>J</i>	$>18.44$
2MASS	<i>H</i>	$>18.26$
2MASS	<i>K</i>	$>17.45$
<i>Euclid</i>	<i>Y</i>	$18.96 \pm 0.01$
<i>Euclid</i>	<i>J</i>	$18.87 \pm 0.01$
<i>Euclid</i>	<i>H</i>	$18.72 \pm 0.01$
WISE	<i>W1</i>	$19.22 \pm 0.24$
WISE	<i>W2</i>	$18.76 \pm 0.32$
WISE	<i>W3</i>	$19.03 \pm 0.48$
WISE	<i>W4</i>	$>17.44$

**Table 2.** Photometry of the host galaxy of AT 2024ahzi. All photometry is corrected for dust extinction in the direction of the SN, using the E. F. Schlafly & D. P. Finkbeiner (2011a) dust maps and  $A_V = 0.30^{+0.08}_{-0.07}$ .

tudes. These fluxes should be extremely similar to those extracted directly from *Euclid* images, and therefore do not bias *Prospector*’s SED fitting.

All galaxy images used for photometry extraction were taken well before AT 2024ahzi’s explosion, so there is no risk of flux contamination from the SN itself. We list host magnitudes and upper limits from all sources in Table 2.

To model the stellar population properties of the host, we jointly fit the photometric detections and spectrum with *Prospector* (J. Leja et al. 2019; B. D. Johnson et al. 2021), a Python-based stellar population model-

ing inference code. Sampling and model details can be found in Appendix A. The SED of the best-fit model is shown in Figure 3. We find that the host of AT 2024ahzi has a stellar mass of  $\log(M_*/M_\odot)=9.86^{+0.03}_{-0.03}$ , which is consistent with previous samples of both low-redshift (S. Schulze et al. 2021) and high-redshift (M. Grayling et al. 2023) SN II host galaxies. It also has a star formation rate of  $1.38^{+0.886}_{-0.50} M_\odot \text{ yr}^{-1}$  and specific SFR of  $\log(\text{sSFR}) = -9.8^{+0.10}_{-0.09} \text{ yr}^{-1}$ . These values are typical for SN II host galaxies, as shown in (S. Schulze et al. 2021). We determine that the host lies along the star-forming “main sequence” as defined in J. Leja et al. (2022) and P. Popesso et al. (2022), and is therefore actively star-forming. This is consistent with our classification of AT 2024ahzi as a SN IIP; a quiescent host galaxy would be far less likely to house a core-collapse SN.

Prospector returns a  $V$ -band dust attenuation of  $A_V=0.30^{+0.08}_{-0.07}$  mag, but the effective reddening of AT 2024ahzi’s photometry depends on both the host’s offset and line of sight. Therefore, in the next sections we analyze AT 2024ahzi’s photometry without correcting for host extinction unless otherwise stated.

#### 4. PHOTOMETRIC ANALYSIS

In this section, we discuss all processing and downstream analysis of AT 2024ahzi’s DECam and ComCam photometry.

There are 187 *griz*-band observations of AT 2024ahzi in the combined ComCam-DECam photometry. We convert the photometry from apparent to absolute magnitudes using  $z_{\text{host}} = 0.202$  and a flat  $\Lambda$ CDM cosmology consistent with the Planck 2015 results (Planck Collaboration et al. 2016). We also phase the light curve around peak, and correct the time axis for time dilation. We treat ComCam and DECam observations in the same passband as from a single instrument; this is a fair assumption since they share similar filter profiles and overlap in their photometry (as shown in Figure 2).

Additionally, we correct for Milky Way extinction using the dust maps provided by D. J. Schlegel et al. (1998) and E. F. Schlafly & D. P. Finkbeiner (2011b), and assuming a E. L. Fitzpatrick & D. Massa (2007) extinction model with  $R_V = 3.1$ . We repeat the following analysis with and without a correction for host extinction, and compare the two sets of results.

##### 4.1. Type IIP Classification and Superphot+ Fitting

Visually, the fast rise and extended plateau of AT 2024ahzi is photometrically consistent with a SN IIP. As a more quantitative measure, we use Superphot+ (K. M. de Soto et al. 2024) to both fit and

classify the light curve of AT 2024ahzi. Superphot+ fits multiband photometry to user-defined parametric models using a suite of samplers and utilizes these parameterized fits for photometric classification.

We fit our light curves jointly across filters (normalized in flux space) using a standard empirical SN model (V. A. Villar et al. 2019, G. Hosseinzadeh et al. 2020), as shown in the left panel of Figure 4. Using the best-fit model values as inputs, we classify AT 2024ahzi using two supernova classifiers from K. M. de Soto et al. (2024) that include and exclude redshift information, respectively. These classifiers yield one of five output labels: SN Ia, SN II (which includes SNe IIP and SNe IIL), SN IIn, SN Ib/c, and SLSN-I. Because the ZTF public surveys only observe in the  $g$ - and  $r$ -bands, we use our fit’s  $g$ - and  $r$ -band parameters for classification. The redshift-agnostic ZTF classifier reports a 92% SN II pseudo-probability, while including peak absolute magnitude as a feature raises the pseudo-probability to 98%. We therefore photometrically classify AT 2024ahzi as a SN II with high confidence. We further subclassify it as a SN IIP from its visually extended plateau, though recent analysis supports a continuum between SNe IIP and SNe IIL over a clear distinction (A. Gal-Yam 2012; P. J. Pessi et al. 2023; V. Morozova et al. 2017; D. Hiramatsu et al. 2021; J. P. Anderson et al. 2014; N. E. Sanders et al. 2015; S. Valenti et al. 2016; L. Galbany et al. 2016).

We note that this is an imperfect classification method, since the classifiers are trained on data from ZTF, and there is a filter mismatch between the ZTF and LSST filters. Furthermore, we do not apply a  $K$ -correction to account for the wavelength shift between the emitted and observed flux distribution. The latter effect is significant, since the ZTF training set is also low redshift ( $z \lesssim 0.1$ ). To highlight the robustness of our classification to  $K$ -corrections, we use AT 2024ahzi’s  $r$ - and  $i$ -band fit parameters as inputs, mimicking the full filter shift in emitted  $gr$ -band flux that would occur if  $z \approx 0.22 - 0.28$ . The classification pseudo-probability decreased to 94% and 87% with and without redshift information, respectively. If we adjust the original  $g$ - and  $r$ -band fit parameters by correcting for host extinction, the pseudo-probabilities are 97% and 95%. Because Superphot+ SN II pseudo-probabilities are underconfident, all of the above pseudo-probabilities correspond to calibrated confidences  $> 99\%$ . Therefore, we conclude that our SN II classification for AT 2024ahzi is robust to both redshift effects and host-galaxy dust.

In practice, we want to classify Rubin transients as early as possible for timely spectroscopic follow-up. Even when only ComCam (i.e., early-phase) photome-

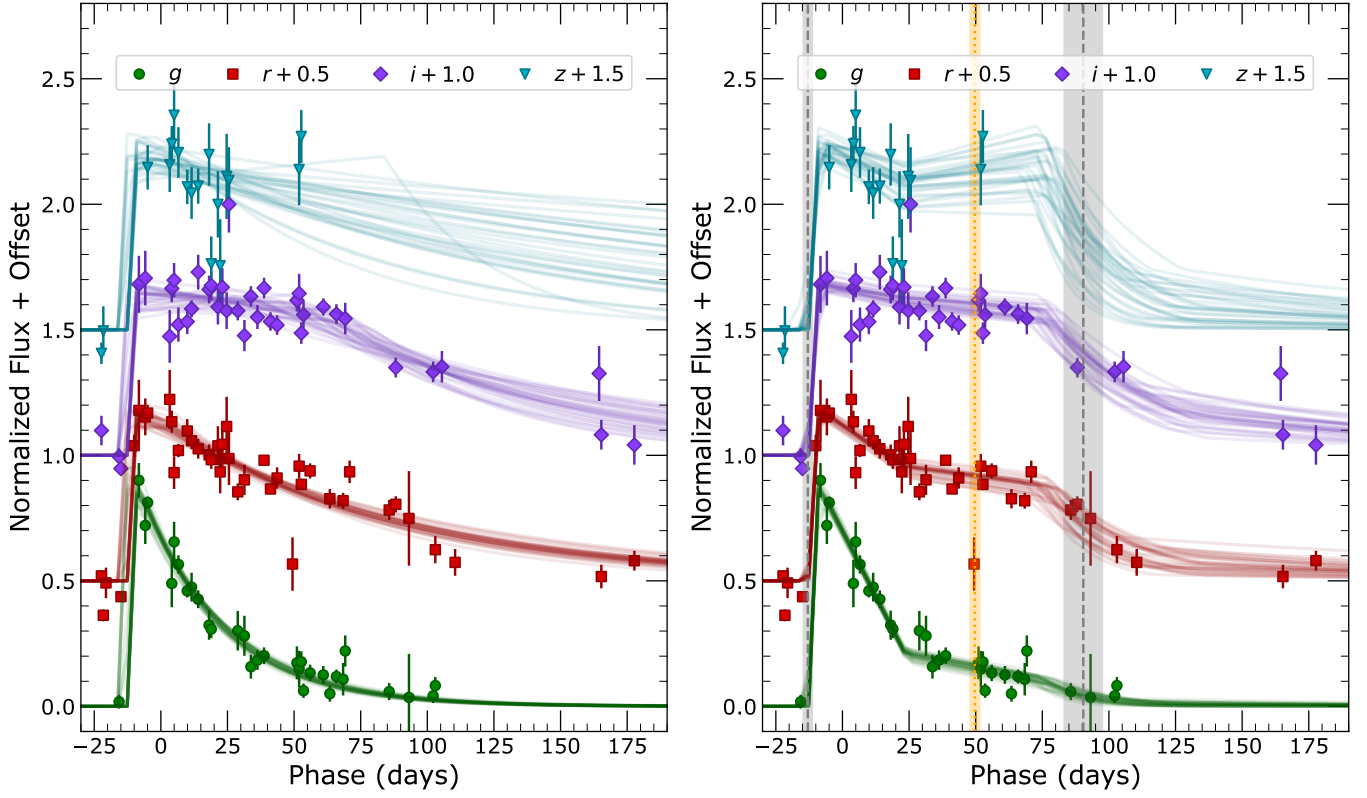


**Figure 4.** *Left:* Superphot+ fit to AT 2024ahzi used for initial classification. Both the redshift-inclusive and redshift-agnostic classifiers assign a SN II label to the best-fit parameter set, with confidences of 98% and 92%, respectively. *Right:* SN IIP-specific Superphot+ fit to AT 2024ahzi. The flat plateau from hydrogen recombination is differentiated from the steeper dimming and cooling region following shock-breakout, possibly lengthened by an extended CSM. We define “plateau duration” as the time from explosion to where the flux drops halfway after hydrogen recombination, as bounded by the vertical gray dashed lines. We measure the plateau magnitude and color from midway along the hydrogen recombination region (dotted yellow line)

try is used for fitting and classification, Superphot+ still labels AT 2024ahzi as a SN II, albeit with lower confidence. A modified classifier trained only on early-phase fit features (see Section 5.2 of K. M. de Soto et al. 2024) returns a SN II prediction with 63% pseudo-probability (90% calibrated confidence) with redshift information and 53% pseudo-probability (84% calibrated confidence) without redshift information. This suggests that SNe II can be discerned at very early phases from their fast rise timescales (S. Gonzalez-Gaitan et al. 2015; A. Gal-Yam et al. 2022).

After using the general SN model fit to classify AT 2024ahzi, we refit the photometry to a parametric model specifically designed for SNe IIP, fitting a steeper, shock cooling component preceding the shallower recombination plateau (K. de Soto in prep.):

$$F(\phi) = \frac{A}{1 + e^{-\phi/\tau_{\text{rise}}}} \times \begin{cases} 1 - (\beta_1 + \beta_2)\phi, & \text{if } \phi < \gamma_1 \\ 1 - \beta_1\gamma_1 - \beta_2\phi, & \text{if } \gamma_1 \leq \phi < \gamma_2 \\ C \exp\left[\frac{\gamma_2 - \phi}{\tau_{\text{fall}}}\right], & \text{if } \gamma_2 \leq \phi < \gamma_{\text{cobalt}} \\ C \exp\left[\frac{\gamma_2 - \gamma_{\text{cobalt}}}{\tau_{\text{fall}}}\right] \times \exp\left[\frac{\gamma_{\text{cobalt}} - \phi}{\tau_{\text{cobalt}}}\right], & \text{if } \phi > \gamma_{\text{cobalt}} \end{cases} \quad (1)$$

Here,  $F(\phi)$  is the normalized flux in each band,  $\phi$  is a phase, and  $\tau_{\text{rise}}$ ,  $\tau_{\text{fall}}$ , and  $\tau_{\text{cobalt}}$  are rise, fall, and radioactive decay timescales, respectively. The  $\beta$  and  $\gamma$  parameters correspond to slopes and transition points of each linear decline. The first piecewise component represents the initial rise and dip, the second component corresponds to the shallower plateau region, the third component corresponds to the post-plateau brightness

decline, and the last component is the cobalt decay tail. This is similar to the functional form found in K. M. de Soto et al. (2024), but now there is differentiation between a steeper post-rise decline ( $\beta_1$  and  $\gamma_1$ ), a shallower plateau ( $\beta_2$  and  $\gamma_2$ ), and a radioactive decay tail ( $\beta_{\text{cobalt}}$ ). This model is used to fit each band separately, but joint priors ensure that the piecewise turning points agree across filters. The best fit to the model is shown in the right panel of Figure 4. To determine whether the added SN IIP-specific model parameters improve the fit to a statistically significant degree, we calculate the Bayesian information criterion (BIC) for both the simpler classification model and the SN IIP-specific model. A lower BIC indicates that extra degrees of freedom (i.e. more complex models) are sufficiently improving the fit. The SN IIP fit has a BIC of 149, while the classification SN fit has a BIC of 174. Therefore, we conclude that a parametrization which includes both a steeper and shallower linear region is needed to effectively fit AT 2024ahzi’s photometry. This suggests an extended (possibly CSM) component around AT 2024ahzi’s progenitor, as CSM-ejecta interaction is expected to produce early, blue emission.

From the IIP-specific fit, we extract a plateau duration of  $103.4 \pm 7.3$  days. For this analysis, we define the plateau duration as the time from explosion to midway between plateau end and cobalt tail (e.g., see S. Valenti et al. 2016 and J. A. Goldberg et al. 2019), indicated by the dashed gray lines in the right panel of Figure 4. Note that this differs from both the OPTd and Pd definitions in J. P. Anderson et al. (2014) and C. P. Gutiérrez et al. (2017) but is equivalent to the ‘optd’ defined in L. Martínez et al. (2022c). The latter argues that plateau duration as defined here is more strongly correlated with hydrogen envelope mass than other definitions.

We also extract a mid-plateau  $r$ -band absolute magnitude of  $-17.39 \pm 0.09$  mag. We apply a  $K$ -correction to this magnitude after estimating the temperature evolution in Section 4.2.

#### 4.2. Bolometric Evolution

We use the IIP Superphot+ fit to interpolate AT 2024ahzi’s multi-band light curve. From this interpolated photometry, we estimate AT 2024ahzi’s bolometric evolution using the code `extrab01` (I. Thornton et al. 2024), which approximates the SN IIP photosphere during rise and plateau as an evolving blackbody (see e.g. R. P. Kirshner & J. Kwan 1974; R. G. Eastman et al. 1996 for caveats regarding flux dilution), and fits each epoch of its multiband photometry to a Planck function. When we jointly fit  $griz$ -band data, we recover an effective temperature of  $T_{\text{eff}} \approx 11000$  K and photospheric ra-

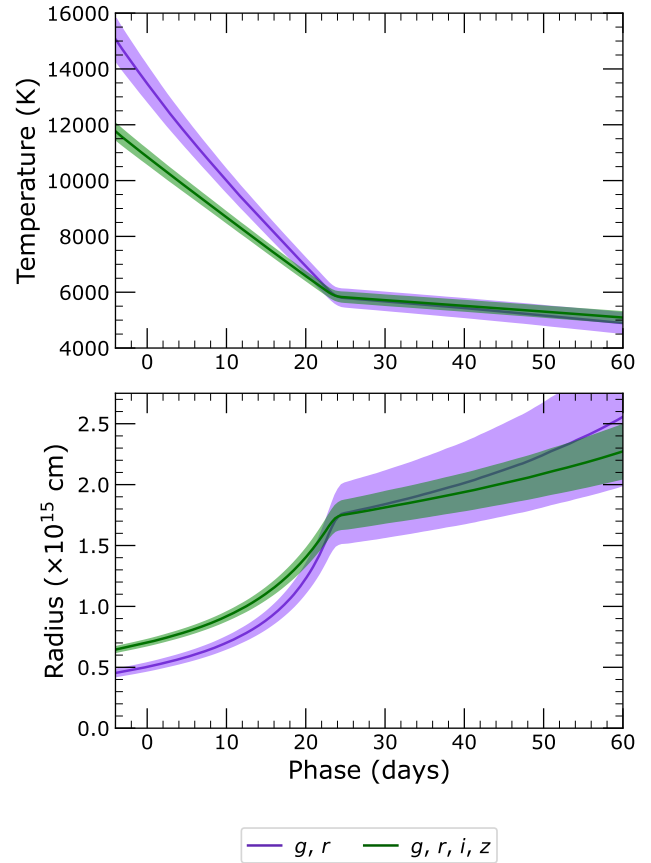


**Figure 5.** Blackbody evolution of AT 2024ahzi, as fit by `extrab01`, using both  $griz$ - and only  $gr$ -band data. The two fits agree along the plateau but differ at early times, a bias that persists after adjusting for host extinction.

dius of  $R_{\text{phot}} \approx 5 \times 10^{14}$  cm at peak. Along the plateau, we recover  $T_{\text{eff}} \approx 6000$ K, which matches the recombination temperature for hydrogen, and  $R_{\text{phot}} \approx 2 \times 10^{15}$  cm. This plateau temperature rules out the possibility of AT 2024ahzi being a SN IIn, which is important to keep in mind when studying its early-phase evolution in Section 4.3.

We also fit an evolving blackbody using only  $g$ - and  $r$ -band data, which is compared to the four-band fit in Figure 5. The two fits align closely along the plateau, but the  $gr$ -fit estimates higher temperatures at early phases. This offset remains even when the photometry is corrected for host extinction. We can attribute this offset to a slight excess of  $iz$ -flux; since all observations lie in the blackbody tail for these temperatures, slight flux excesses can dramatically shift the extracted temperature and radius. This is a trend also seen in T. Faran et al. (2017) and explained by N. Tominaga et al. (2011) and T. Shussman et al. (2016); higher-frequency

photons probe deeper and therefore hotter layers of the ejecta.

Using the effective temperature evolution derived from the `extrabol` fit, we estimate  $K$ -corrections assuming  $z = 0.211$  and a blackbody SED, propagating uncertainties in both temperature and redshift.

### 4.3. Progenitor and CSM Characterization

A supernova’s photometry reveals information about the progenitor that exploded, as well as the CSM surrounding it at the time of explosion. Observed photometry can be cross-matched with a grid of modeled light curves to infer the progenitor, explosion, and CSM properties (e.g., V. Morozova et al. 2017; J. J. Eldridge et al. 2019; D. Hiramatsu et al. 2021; B. L. Barker et al. 2022; L. Martinez et al. 2022c; T. J. Moriya et al. 2023). However, various progenitor configurations can yield statistically identical light curves, though many such configurations are ruled out by stellar evolution models that assume a unique mapping from progenitor radius to ejecta mass (D. Kasen & S. E. Woosley 2009; L. Dessart & D. J. Hillier 2019; J. A. Goldberg et al. 2019; J. Goldberg & L. Bildsten 2020; L. Dessart & W. V. Jacobson-Galán 2023; B. Hsu et al. 2024; Q. Fang et al. 2025; Q. Fang et al. 2025c). For example, the progenitor models in the T. J. Moriya et al. (2023) grid are obtained from T. Sukhbold et al. (2016) and are characterized solely by one of five zero-age main sequence (ZAMS) masses ( $M_{\text{ZAMS}}/M_{\odot} \in \{10, 12, 14, 16, 18\}$ ), where solar metallicity is assumed, and therefore an implicit relation between pre-explosion envelope mass and progenitor radius is established.

To constrain the degeneracy in progenitor and explosion properties for AT 2024ahzi without introducing biases from a model grid, we plug its plateau duration and mid-plateau luminosity ( $L_{\text{plat}} = 2.48 \times 10^{42}$  erg/s, extracted from the blackbody fit) into the analytic scalings from J. A. Goldberg et al. (2019) and J. Goldberg & L. Bildsten (2020):

$$\log L_{\text{mid}} = 42.16 - 0.40 \log M_{10} + 0.74 \log E_{51} + 0.76 \log R_{500} \quad (2)$$

$$\log t_p = 2.184 + 0.134 M_{\text{Ni}} + 0.411 \log M_{10} - 0.282 \log E_{51} \quad (3)$$

These scalings relate progenitor radius ( $R_{500} = R_0/500R_{\odot}$ ), H-rich ejecta mass ( $M_{10} = M_{\text{ej}}/10M_{\odot}$ ), and combined kinetic and radiative explosion energy ( $E_{51} = E_{\text{exp}}/10^{51}$  erg), for a specified nickel mass  $M_{\text{Ni}}$ . We set  $M_{\text{Ni}} = 0.1M_{\odot}$  in accordance with the  $M_{\text{Ni}} - L_{50}$  relation derived in T. Müller et al. (2017), satisfying the

$M_{\text{Ni}} \gtrsim 0.03M_{\odot}$  criterion assumed by the scalings. The two plateau properties define a curve in radius-mass-energy space rather than a single set of values. J. A. Goldberg et al. (2019) estimates a  $\sim 15\%$  theoretical uncertainty in values extracted from this curve.

Considering the broad range of potential progenitor radii supported by S. de Wit et al. (2024) of  $250R_{\odot}$  to  $1750R_{\odot}$ , the possible H-rich ejecta mass and explosion energy range from  $1.58 - 12.13M_{\odot}$  and  $(0.16 - 2.6) \times 10^{51}$  erg, respectively. Specifically, larger values for the progenitor radius correspond to lower inferred H-rich ejecta masses and explosion energies. An independent constraint on progenitor radius is needed to better constrain H-rich ejecta mass and explosion energy. Direct progenitor observation (S. D. V. Dyk 2025) or a measurement of its variability (B. Hsu et al. 2024) is only possible for nearby systems (distance  $\lesssim 30$  Mpc). We can potentially constrain progenitor luminosity from nebular spectra (Q. Fang et al. 2025a,b), which requires spectroscopic follow-up. In the absence of direct or spectroscopic constraints, as will be the case for most Rubin transients, early ( $\lesssim 15$  days after explosion) estimates of photospheric velocity may constrain explosion energy in the absence of CSM interaction (J. A. Goldberg et al. 2019; L. Dessart et al. 2010). For events affected by CSM, we can still constrain families of progenitor and explosion properties, which is useful for ruling out invalid stellar evolution or explosion models.

The prevalence and diversity of CSM around SNe IIP remain an open question (O. Yaron et al. 2017; I. Irani et al. 2024; W. V. Jacobson-Galán et al. 2024; K. R. Hinds et al. 2025), but its impact on optical emission tends to be restricted to early phases ( $\lesssim 40$  days; R. J. Bruch et al. 2023). To explore possible CSM interaction affecting AT 2024ahzi’s early-phase photometry, we fit the photometry to the grid of synthetic SN II models from T. J. Moriya et al. (2023). While this grid has limited progenitor diversity, the early lightcurve is mostly dependent on CSM interaction and thus can more likely be well-represented by the grid’s extensive CSM parameter space. The stars are exploded using STELLA (S. I. Blinnikov et al. 1998), a one-dimensional hydrodynamics code with multi-group radiative transfer. Explosions are modeled across ten explosion energies ( $E_{\text{exp}}/(10^{51} \text{ erg}) \in \{0.5, 1, \dots, 4.5, 5\}$ ) and nine nickel masses ( $M_{\text{Ni}}/M_{\odot} \in \{0.001, 0.01, 0.02, 0.04, 0.06, 0.08, 0.1, 0.2, 0.3\}$ ), uniformly mixed to half the H envelope mass.

The CSM density profile is parameterized by an accelerating wind model, defined as:

$$\rho_{CSM}(r) = \frac{\dot{M}}{4\pi v_{\text{wind}}(r)r^2} \quad (4)$$

$$v_{\text{wind}}(r) = v_0 + (v_\infty - v_0) \left(1 - \frac{R_0}{r}\right)^\beta. \quad (5)$$

Here,  $\beta \in \{0.5, 1, \dots, 4.5, 5\}$  is a shape parameter that controls wind acceleration,  $R_{\text{CSM}} \in \{1, 2, 4, 6, 8, 10\} \times 10^{14}$  cm is the CSM upper radius, and  $\log_{10} \dot{M} \in \{-5, 4.5, \dots, -1.5, -1\} M_\odot/\text{yr}$  is the stellar mass loss rate; all models assume a constant mass-loss rate, and this lost mass forms the CSM. The parameters  $R_0$  and  $v_0$  are the progenitor radius and CSM velocity at the progenitor radius, where  $v_0$  is chosen to maintain a continuous density profile at the progenitor-CSM interface. The asymptotic CSM velocity is set to  $v_\infty = 10$  km/s to reflect wind velocities found around nearby RSGs (J. T. van Loon et al. 2001; S. R. Goldman et al. 2016).

Using the SEDs from T. J. Moriya et al. (2023), we generate apparent multi-band Rubin light curves at  $z = 0.211$  to compare with the observed AT 2024ahzi photometry. To save compute, we only generate redshifted light curves for 81,842 out of the 228,016 total SEDs. We first generated light curves for a coarser distribution of parameters, then iteratively expanded the finer grid around the best-fit models until the fit quality sufficiently declined. Because the explosion time of the modeled light curve may not exactly agree with the explosion time inferred from the optical photometry, we allow for a phase dither of  $\pm 20$  days to best optimize the fit. We find that many models fail to replicate both the CSM-affected (early-phase) and plateau regions. As a result, we separately fit the model grid to the  $\phi < 40$  and  $\phi > 40$  subsets of AT 2024ahzi’s *griz*-photometry, where  $\phi$  is the number of days after explosion. We call these the “early-phase” and “late-phase” fits, respectively. We only consider models with chi-squared values within 20% of the minimum for *both* fits. This ensures good agreement along the SN’s entire evolution. 46 models pass this criteria, each with combined reduced chi-squared  $3.2 < \chi_{\text{red}}^2 < 3.8$ . The early-phase fits have  $4.6 < \chi_{\text{red}}^2 < 5.5$ , and are statistically worse than the late-phase fits, which have  $2.0 < \chi_{\text{red}}^2 < 2.3$ . Relaxing the reduced chi-squared cut to within 50% of the minimum increases the well-fit set to 310 models. This keeps all parameter distributions approximately the same, except it extends the range of well-fit ZAMS masses.

Within the 46 well-fit models, all have  $E_{\text{exp}} = 10^{51}$  ergs and 96% have  $M_{\text{ZAMS}} = 12 - 14M_\odot$ , which corresponds to  $M_{\text{H,ej}} = 7.8 - 8.1M_\odot$ . The remaining have  $M_{\text{ZAMS}} = 10M_\odot$  or  $16M_\odot$ , and these masses become

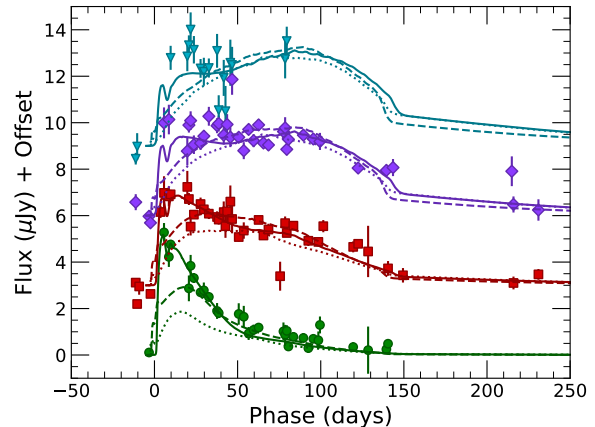


**Figure 6.** Optimal CSM model (solid line) from T. J. Moriya et al. (2023), found among the models well-fit within both the early ( $\phi < 40$  days) and late ( $\phi > 40$  days) phases of 2024ahzi’s photometry. We compare to the best CSM-less model (dashed), and the best CSM model but with the CSM removed (dotted). Both CSM-less fits are poor relative to the best CSM fit, highlighting how CSM must be added to the T. Sukhbold et al. (2016) stellar profiles to replicate AT 2024ahzi’s photometry. The best CSM fit favors a low mass-loss rate but slow wind acceleration, which is effectively indistinguishable from an extended stellar profile at the photosphere.

more prevalent when extending the reduced chi-squared cutoff. The fit nickel masses are between  $0.06 - 0.1M_\odot$ , which matches the  $M_{\text{Ni}} = 0.1M_\odot$  assumption we made when deriving the J. A. Goldberg et al. (2019) scalings. The model grid intersects the radius-mass-energy curve we derived above at  $M_{\text{ZAMS}}$  between  $12M_\odot$  and  $14M_\odot$  and  $E_{\text{exp}}$  between  $(1 - 1.5) \times 10^{51}$  ergs. Therefore, our best-fit T. J. Moriya et al. (2023) models are consistent with the derived J. A. Goldberg et al. (2019) scalings.

The majority of well-fit models have slow wind acceleration and moderate mass loss rates; 89% have  $\beta \geq 2.5$  and  $-2.5 \leq \log_{10} \dot{M} \leq -1.5$ . This aligns with the results of J. Silva-Farfán et al. (2024) using the T. J. Moriya et al. (2018) model grid. There is not a strong preference for  $R_{\text{CSM}}$ , but a coefficient of determination of  $R^2 = 0.9$  indicates that larger CSM radii strongly correlate with lower mass loss rates.

For each well-fitting model, we calculate the total CSM mass  $M_{\text{CSM}}$  using Equations 1 and 2 from T. J. Moriya et al. (2023) and:

$$\begin{aligned}
M_{\text{CSM}} &= 4\pi \int_{R_0}^{R_{\text{CSM}}} \rho(r) r^2 dr \\
&= \dot{M} \int_{R_0}^{R_{\text{CSM}}} v_{\text{wind}}^{-1}(r) dr \\
&= \dot{M} \int_{R_0}^{R_{\text{CSM}}} \left[ v_0 + (v_\infty - v_0) \left(1 - \frac{R_0}{r}\right)^\beta \right]^{-1} dr
\end{aligned} \tag{6}$$

Before constraining AT 2024ahzi’s CSM mass, we first argue that AT 2024ahzi’s early-phase photometry cannot be well-fit without an extended, CSM-like density profile. To show this, we consider only models with  $M_{\text{CSM}} < 10^{-2.5} M_\odot$  as a proxy for CSM-less models, in accordance with [K. R. Hinds et al. \(2025\)](#). The best CSM-less model has higher progenitor mass (ZAMS =  $16M_\odot$ ) than the best CSM model, with  $\chi_{\text{red}}^2 = 12.3$  for  $\phi < 40$  days and  $\chi_{\text{red}}^2 = 7.3$  for the full light curve. This translates to a BIC of 1020 for the full light curve; when we add CSM, the lowest BIC is 475. Therefore, we conclude that the CSM parameters are needed to adequately model AT 2024ahzi’s photometry, at least within the model grid used.

The best-fit CSM model, which minimizes the combined chi-squared value within our “well-fit” set, has  $M_{\text{ZAMS}} = 12M_\odot$ ,  $E_{\text{exp}} = 10^{51}$  ergs,  $M_{\text{Ni}} = 0.1M_\odot$ ,  $\beta = 4.5$ ,  $\dot{M} = 10^{-2} M_\odot/\text{yr}$ ,  $R_{\text{CSM}} = 4 \times 10^{14}$  cm, and  $M_{\text{CSM}} = 1.4M_\odot$ . The corresponding model fit is shown in [Figure 6](#).

For all well-fit models,  $M_{\text{CSM}}$  ranges from 0.7 to 2.1 solar masses. These are values typical of SNe IIn rather than SNe II ([C. L. Ransome & V. A. Villar 2025](#)), and is on the very upper end of the CSM mass derived from [K. R. Hinds et al. \(2025\)](#). Because AT 2024ahzi’s effective temperature remains near 6000K for the entirety of the plateau region, it is unlikely to be a misclassified SN IIn. We conclude that either (1) CSM mass estimates are highly sensitive to the assumed CSM density prescription, and we have made assumptions different to previous works or (2) we are overestimating the mass by assuming all is detached from the progenitor. To support the former, we note that since we assume an accelerating wind, the degree of that wind acceleration dramatically affects the estimated CSM mass using [Equation \(6\)](#). In contrast, [K. R. Hinds et al. \(2025\)](#) calculates  $M_{\text{CSM}}$  assuming constant wind velocity (i.e. assuming  $\beta = 0$  and  $v_{\text{wind}} = v(R_{\text{CSM}})$ ):

$$M_{\text{CSM,approx}} = \frac{\dot{M} R_{\text{CSM}}}{v(R_{\text{CSM}})} \tag{7}$$

$$= \frac{\dot{M} R_{\text{CSM}}}{v_0 + (v_\infty - v_0) \left(1 - R_0/R_{\text{CSM}}\right)^\beta} \tag{8}$$

Plugging our CSM values into this equation yields CSM masses between 0.1 and  $0.8 M_\odot$ , which is far less anomalous compared to that paper’s distribution. This highlights how large  $\beta$  values can increase total CSM mass by a factor of ten by significantly slowing down the CSM wind and increasing its density.

Alternatively, we may be overestimating AT 2024ahzi’s CSM mass if we are instead probing an extended, static progenitor envelope closely resembling a slowly-accelerating CSM ([L. Dessart et al. 2017](#)). Because the [T. Sukhbold et al. \(2016\)](#) progenitors all have an exponential density profile, a massive “CSM” density profile may be mimicking a greater underlying diversity in progenitor envelopes. To support this hypothesis, we only consider the CSM mass above the photosphere at time of explosion, as is the convention in [B. Davies et al. \(2022\)](#). We recover a photosphere radius of  $9 \times 10^{13}$  cm ( $\approx 1300R_\odot$ ), which is double the stated progenitor radius, and a total mass of  $0.4M_\odot$  above the photosphere. Additionally, the photospheric wind velocity is only 0.6 km/s, far lower than narrow line velocities observed in early phases of SNe II with CSM interaction ([W. V. Jacobson-Galán et al. 2022](#)). These negligible velocities could instead be interpreted as a more extended hydrostatic envelope, which transitions to a true wind much farther out.

While previously large RSGs have been observed in the past, this radius seems incompatible with a  $12M_\odot$  ZAMS evolutionary track ([E. M. Levesque et al. 2005](#)). Furthermore, modeled RSG radii are likely already larger than physically viable ([L. Dessart et al. 2013](#)), so a radius that further exceeds the modeled value seems unlikely.

We can reconcile our findings with these previous works by extending the progenitor model grid and relaxing the assumed relation between ejecta mass and progenitor radius in the [T. Sukhbold et al. \(2016\)](#) models. From the [J. A. Goldberg et al. \(2019\)](#) relations, a lower ejecta mass, smaller radius, and higher explosion energy should leave the plateau duration and luminosity unchanged. Following the light-CSM peak luminosity scalings of [D. Khatami & D. Kasen \(2024\)](#), a higher explosion energy lowers the CSM mass needed to replicate the early-phase luminosity peak. Therefore, revised models with smaller progenitor radii may simultaneously better align with previous findings and lower estimated CSM masses to more closely match those of other SNe IIP.

## 5. AT 2024AHZI IN CONTEXT

We compare the plateau properties of AT 2024ahzi to a broader sample of SNe IIP presented in [K. de Soto](#)

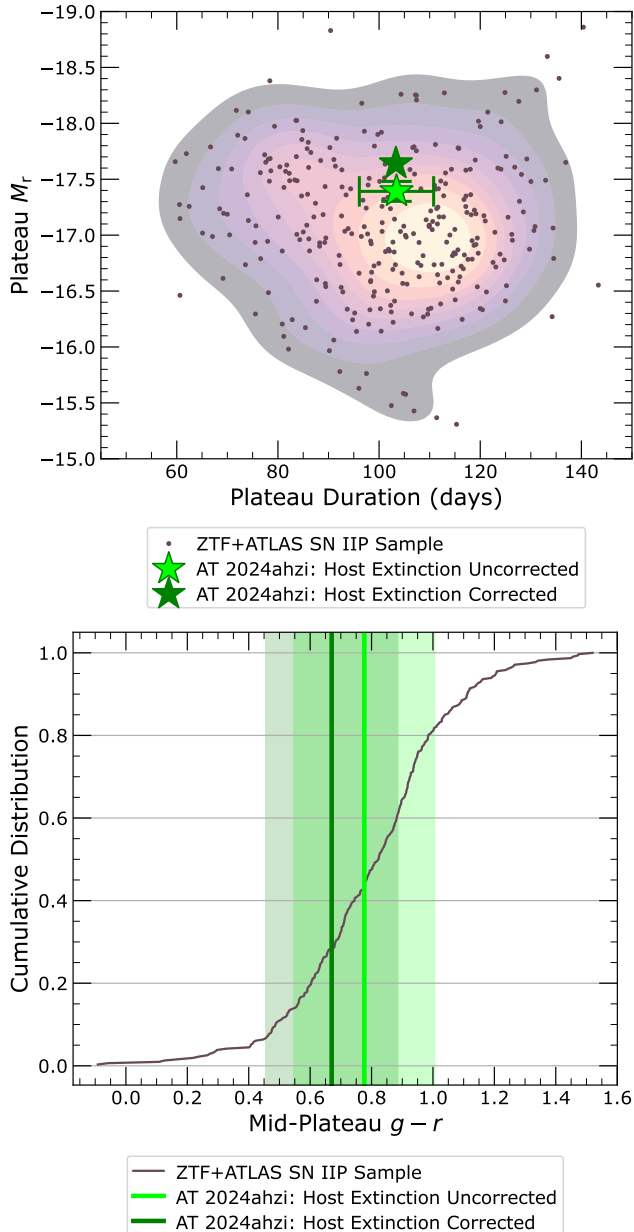


**Figure 7.** *Top:* AT 2024ahzi’s plateau duration and  $r$ -band absolute magnitude, as fit by Superphot+, compared to those of the ZTF-ATLAS SN IIP sample. A blackbody  $K$ -correction is used to adjust AT 2024ahzi’s plateau. Both correcting (dark green) and not correcting (lime green) for host extinction yields values well within the norm for the SN IIP sample. *Bottom:* 2024ahzi’s mid-plateau,  $K$ -corrected,  $g-r$  color compared to the sample’s cumulative distribution, before (dark green) and after (light green) correcting for host-galaxy extinction. Both  $g-r$  colors are near the median for the sample.

(in prep.). The sample consists of 313 spectroscopically identified SNe IIP with high-quality photometric coverage from ZTF and ATLAS, with likely non-SNe IIP re-

moved via photometric cuts. The sample is low-redshift, with 90% of the events having  $z < 0.05$  and every event being closer than AT 2024ahzi. The ZTF-ATLAS sample is fit hierarchically to the SN IIP Superphot+ model presented in Sec. 4.1.

In the top panel of Figure 7, we plot the rest-frame (e.g. corrected for time dilation) plateau duration and mid-plateau  $r$ -band magnitude of AT 2024ahzi against those of the larger ZTF-ATLAS sample. In the bottom panel, we compare mid-plateau  $g-r$  colors. This is not a perfect comparison, however, as the Rubin  $g$  and  $r$  filter profiles are somewhat wider and slightly closer together than those from Palomar. All three of AT 2024ahzi’s plateau properties are within 25% of the median from the ZTF-ATLAS sample (i.e. within the interquartile range). Despite its higher redshift, AT 2024ahzi is clearly an observationally typical Type IIP SN.

Correcting for the  $A_V \approx 0.30$  mag host extinction from Section 3 moves AT 2024ahzi’s plateau properties farther from the center of the larger SN IIP distribution. The plateau  $r$ -band absolute magnitude is brighter than 66% of the ZTF-ATLAS sample without host extinction correction, and 81% after host extinction correction. Similarly, the  $g-r$  color goes from being bluer than 57% of the sample to 72% of the sample after correcting for host extinction. This correction could be an overestimate, since AT 2024ahzi is located on the outskirts of its host galaxy. We note high uncertainties in AT 2024ahzi’s color estimates, propagated from uncertainties in both photometric redshift and  $g$ -band plateau magnitude.

We do not compare AT 2024ahzi’s blackbody evolution to that of the ZTF-ATLAS sample, as `extrabotl`’s predictions with four-band differs from its prediction using only  $gr$ -band data, skewing comparison with  $gr$ -band ZTF-ATLAS fits.

We expect LSST SNe II to have redshifts similar to that of AT 2024ahzi (R. Kessler et al. 2019), so the LSST SN IIP sample will be of consistently higher redshift than the ZTF-ATLAS sample. This means that the context surrounding AT 2024ahzi may change as we gather a new comparison dataset. We therefore plan on applying a similar analysis to future LSST SNe II to quantify shifts in plateau property distributions with redshift, if any.

## 6. CONCLUSIONS AND SUMMARY

In this paper we present joint Rubin ComCam and DECam photometry for AT 2024ahzi. We associate AT 2024ahzi to a nearby star-forming host, which allows us to estimate the SN’s redshift and dust extinction. We interpolate and photometrically classify AT 2024ahzi as

a SN IIP with  $> 99\%$  calibrated confidence using Superphot+, making it the first photometrically classified SN II observed by Rubin ComCam. Because we use deep DES template images to re-extract forced photometry from ComCam images, we can strongly constrain both the brightening timescale and early color evolution of the AT 2024ahzi’s light curve. This results in a confident multi-band fit and classification, even using only early-phase ComCam data. By analyzing AT 2024ahzi’s multiband and blackbody evolution and comparing it to a larger population of low-redshift SNe IIP, we determine that its properties are typical of previously observed, lower-redshift SN IIP. Applying a similar analysis pipeline to the larger expected sample of LSST SNe IIP will allow us to establish trends between SN IIP light curve and progenitor properties, and quantify associated scatter with higher precision. Rather than extracting a single optimal progenitor mass and radius, we constrain a family of possible progenitor properties from the extracted plateau properties. Population progenitor analysis from many SNe II will help us rule out models with radius-mass-energy combinations outside of the joint degeneracy curve. Finally, we fit AT 2024ahzi’s early-phase photometry to a grid of CSM models and estimate a CSM mass of  $0.4M_{\odot}$  above the photosphere. Our fits favor slow wind acceleration in the CSM, which can alternately be explained by an extended progenitor density profile.

Rubin is expected to discover approximately one million new transients per year (J. Tyson 2002; R. Kessler et al. 2019; M. L. Graham et al. 2024). Through this analysis, we outline a pipeline for identifying, processing, and studying potential SNe II within this dataset for subsequent population studies. Because we probabilistically associate events with host galaxies, we can photometrically estimate redshift and therefore use absolute magnitude information in classification without spending limited spectroscopic resources. Our resulting dataset of photometrically classified SNe II will elucidate the significance of the red supergiant problem (S. J. Smartt et al. 2009; S. J. Smartt 2015) and the prevalence of eruptive or wind-like CSM (V. Morozova et al. 2018; B. Davies et al. 2022; T. Matsumoto & B. D. Metzger 2022). Early-phase classification and modeling of SNe II will allow us to rapidly follow up on those with evidence of CSM interaction; we aim to capture CSM flash features in the resulting pre-peak spectroscopy (C. S. Kochanek 2018; W. V. Jacobson-Galán et al. 2022; L. Dessart & W. V. Jacobson-Galán 2023).

This work highlights how observing facilities beyond Rubin can supplement Rubin photometry through simultaneous observation, effectively increasing the ob-

serving cadence. This supplementary data becomes necessary for classification when Rubin does not capture an event’s full light curve evolution. Analysis of AT 2024ahzi’s plateau properties is only possible with both ComCam and DECam photometry. Surveys from DECam, ZTF, YSE (through the Pan-STARRS telescopes; K. C. Chambers et al. 2016), the *Nancy Grace Roman Space Telescope* High Latitude Time Domain Survey (HLTDS; B. M. Rose et al. 2021), and the La Silla Schmidt Southern Survey (LS4; A. A. Miller et al. 2025), among others, will maximize the science gleaned from transients discovered by Rubin.

#### ACKNOWLEDGMENTS

The Villar Astro Time Lab acknowledges support through the David and Lucile Packard Foundation, the Research Corporation for Scientific Advancement (through a Cottrell Fellowship), the National Science Foundation under AST-2433718, AST-2407922 and AST-2406110, as well as an Aramont Fellowship for Emerging Science Research. K.d.S. and C.T.M. thank the LSST-DA Data Science Fellowship Program, which is funded by LSST-DA, the Brinson Foundation, the WoodNext Foundation, and the Research Corporation for Science Advancement Foundation; their participation in the program has benefited this work. J.A.G. acknowledges financial support from NASA grant 23-ATP23-0070. The Flatiron Institute is supported by the Simons Foundation. The UCSC team is supported in part by NSF grant AST-2307710 and by a fellowship from the David and Lucile Packard Foundation to R.J.F. T.G. is a Canadian Rubin Fellow at the Dunlap Institute. The Dunlap Institute is funded through an endowment established by the David Dunlap family and the University of Toronto. L.I. acknowledges financial support from the INAF Data Grant Program ‘YES’ (PI: Izzo) *Multi-wavelength and multi messenger analysis of relativistic supernovae*. D.A.C. acknowledges funding through *JWST* program grants JWST-GO-06541, JWST-GO-06585, and JWST-GO-05324. C.G. and D.A.F. are supported by a VILLUM FONDEN Villum Experiment grant (VIL69896). D.A.F. and J.H. acknowledge support from a research grant from VILLUM FONDEN (VIL54489). D.A.F. acknowledges support from the VILLUM FONDEN Young Investigator Grant (project number 25501) and VILLUM FONDEN research grant VIL16599. W.B.H. acknowledges support from the NSF Graduate Research Fellowship Program under Grant No. 2236415. D.O.J. acknowledges support from NSF grants AST-2407632, AST-2429450, and AST-2510993, NASA grant 80NSSC24M0023, and

HST/JWST grants HST-GO-17128.028 and JWST-GO-05324.031, awarded by the Space Telescope Science Institute (STScI), which is operated by the Association of Universities for Research in Astronomy, Inc., for NASA, under contract NAS5-26555. G.Nair’s involvement in this work is through membership in the Rubin SITCOM In-Kind Commissioning US/Chile-11 team to coordinate Rubin ComCam and DECam observations during commissioning. G.Narayan is funded by the DOE through the Department of Physics at the University of Illinois, Urbana-Champaign (#13771275), and NSF CAREER grant AST-2239364, supported in-part by funding from Charles Simonyi. G.Narayan also gratefully acknowledges NSF support from OAC-2311355 and AST-2432428, as well as AST-2421845 and funding from the Simons Foundation for the NSF-Simons SkAI Institute, and support from the HST Guest Observer Program through HST-GO-16764, and HST-GO-17128 (PI: R. Foley). G.Narayan and H.P. gratefully acknowledge NSF support from AST-2206195. M.V. acknowledges funding from the Center for Astrophysical Surveys Graduate Fellowship. Q.W. is supported by the Sagol Weizmann-MIT Bridge Program. A.R.W. acknowledges support from the U.S. Department of Energy through the Department of Physics at the University of Illinois, Urbana-Champaign (#13771275). Y.Z. acknowledges support from MAOF grant 12641898 and visitor support from the Observatories of the Carnegie Institution for Science, Pasadena CA, where part of this work was completed.

This work is supported by the National Science Foundation under Cooperative Agreement PHY-2019786 (the NSF AI Institute for Artificial Intelligence and Fundamental Interactions). Parts of this research were supported by the Australian Research Council Centre of Excellence for Gravitational Wave Discovery (OzGrav), through project number CE230100016.

The Young Supernova Experiment (YSE) and its research infrastructure is supported by the European Research Council under the European Union’s Horizon 2020 research and innovation programme (ERC Grant Agreement 101002652, PI K. Mandel), the Heising-Simons Foundation (2018-0913, PI R. Foley; 2018-0911, PI R. Margutti), NASA (NNG17PX03C, PI R. Foley), NSF (AST-1720756, AST-1815935, PI R. Foley; AST-1909796, AST-1944985, PI R. Margutti), the David & Lucille Packard Foundation (PI R. Foley), VILLUM FONDEN (project 16599, PI J. Hjorth), and the Center for Astrophysical Surveys (CAPS) at the National Center for Supercomputing Applications (NCSA) and the University of Illinois Urbana-Champaign.

This project used data obtained with the Dark Energy Camera (DECam), which was constructed by the Dark Energy Survey (DES) collaboration. Funding for the DES Projects has been provided by the US Department of Energy, the U.S. National Science Foundation, the Ministry of Science and Education of Spain, the Science and Technology Facilities Council of the United Kingdom, the Higher Education Funding Council for England, the National Center for Supercomputing Applications at the University of Illinois at Urbana-Champaign, the Kavli Institute for Cosmological Physics at the University of Chicago, Center for Cosmology and Astrophysics at the Ohio State University, the Mitchell Institute for Fundamental Physics and Astronomy at Texas A&M University, Financiadora de Estudos e Projetos, Fundao Carlos Chagas Filho de Amparo à Pesquisa do Estado do Rio de Janeiro, Conselho Nacional de Desenvolvimento Científico e Tecnológico and the Ministério da Ciência, Tecnologia e Inovação, the Deutsche Forschungsgemeinschaft and the Collaborating Institutions in the Dark Energy Survey.

The Collaborating Institutions are Argonne National Laboratory, the University of California at Santa Cruz, the University of Cambridge, Centro de Investigaciones Energéticas, Medioambientales y Tecnológicas Madrid, the University of Chicago, University College London, the DES-Brazil Consortium, the University of Edinburgh, the Eidgenössische Technische Hochschule (ETH) Zürich, Fermi National Accelerator Laboratory, the University of Illinois at Urbana-Champaign, the Institut de Ciències de l’Espai (IEEC/CSIC), the Institut de Física d’Altes Energies, Lawrence Berkeley National Laboratory, the Ludwig-Maximilians Universität München and the associated Excellence Cluster Universe, the University of Michigan, NSF NOIRLab, the University of Nottingham, the Ohio State University, the OzDES Membership Consortium, the University of Pennsylvania, the University of Portsmouth, SLAC National Accelerator Laboratory, Stanford University, the University of Sussex, and Texas A&M University.

Based on observations at NSF Cerro Tololo Inter-American Observatory, NSF NOIRLab (NOIRLab Prop. IDs 2024B-763968, 2024B-441839, and 2025A-388357; PI G. Narayan and A. Rest; 2012B-0001; PI: J. Frieman; 2014B-0404; PIs: D. Schlegel and A. Dey), which is managed by the Association of Universities for Research in Astronomy (AURA) under a cooperative agreement with the U.S. National Science Foundation.

This material is based upon work supported in part by the National Science Foundation through Cooperative Agreements AST-1258333 and AST-2241526 and Coop-

erative Support Agreements AST-1202910 and 2211468 managed by the Association of Universities for Research in Astronomy (AURA), and the Department of Energy under Contract No. DE-AC02-76SF00515 with the SLAC National Accelerator Laboratory managed by Stanford University. Additional Rubin Observatory funding comes from private donations, grants to universities, and in-kind support from LSST-DA Institutional Members.

No proprietary Rubin data is included in this work.

This publication makes use of data products from the Two Micron All Sky Survey, which is a joint project of the University of Massachusetts and the Infrared Processing and Analysis Center/California Institute of Technology, funded by the National Aeronautics and Space Administration and the National Science Foundation.

This work has made use of the Quick Release (Q1) data from the Euclid mission of the European Space

Agency (ESA). [<https://doi.org/10.57780/esa-2853f3b>]  
<https://doi.org/10.57780/esa-2853f3b>].

This publication makes use of data products from the Wide-field Infrared Survey Explorer, which is a joint project of the University of California, Los Angeles, and the Jet Propulsion Laboratory/California Institute of Technology, funded by the National Aeronautics and Space Administration.

*Facilities:* DECam, VRO

*Software:* `astropy` (Astropy Collaboration et al. 2013, 2018, 2022), `Cloudy` (G. J. Ferland et al. 2013), `Source Extractor` (E. Bertin & S. Arnouts 1996), `YSE-PZ` (D. A. Coulter et al. 2022; D. A. Coulter et al. 2023), `Superphot+` (K. M. de Soto et al. 2024)

## APPENDIX

### A. PROCEDURE FOR PROSPECTOR MODELING AND FITTING

`Prospector` determines posterior distributions for galactic properties using the `dynesty` (J. S. Speagle 2020) nested sampling fitting routine, and produces model spectra and photometry using `FSPS` and `python-FSPS` (C. Conroy et al. 2009; C. Conroy & J. E. Gunn 2010). Internally, `Prospector` uses `MIST` models (B. Paxton et al. 2018) and `MILES` spectral libraries (J. Falc3n-Barroso et al. 2011). Our `Prospector` model includes the P. Kroupa & T. Jerabkova (2021) initial mass function (IMF), a nebular emission model (N. Byler et al. 2017), and the B. T. Draine & A. Li (2007) IR dust emission model. To measure dust attenuation in the host, we use the M. Kriek & C. Conroy (2013) dust emission model, which applies an offset to the D. Calzetti et al. (2000) dust attenuation curve and determines the optical depth of light attenuated from old and young stellar light. To ensure that only realistic combinations of total mass formed in the galaxy ( $M_F$ ) and stellar metallicity ( $Z_*$ ) are sampled, we constrain these properties with the A. Gallazzi et al. (2005) mass-metallicity relation. We further employ non-parametric star formation history (SFH) model with seven age-bins: the first two are linearly spaced from 0-30 Myr and 30-100Myr, and the last five are log-spaced until the age of the Universe at  $z = 0.211$ . Finally, we apply several parameters to fit the host spectrum: a spectral smoothing model, which normalizes the spectrum to the host photometry, a gas-phase metallicity, which is dependent on the host’s spectral line strengths, a template to marginalize over the observed nebular emission lines, a noise inflation model that ensures the spectrum is not overweighted in the fit compared to the photometry, and a pixel outlier model to marginalize over spectral noise.

We use the best-fit SFH and  $M_F$  to calculate a stellar mass ( $M_*$ ), mass-weighted stellar population age ( $t_m$ ), and present-day star formation rate (SFR). We further convert the optical depth of dust attenuated from old and young stellar light to a  $V$ -band dust extinction in magnitudes ( $A_V$ ).

## REFERENCES

- Abbott, T. M. C., Adam3w, M., Agüena, M., et al. 2021, *ApJS*, 255, 20, doi: [10.3847/1538-4365/ac00b3](https://doi.org/10.3847/1538-4365/ac00b3)
- Adams, S. M., Kochanek, C. S., Gerke, J. R., Stanek, K. Z., & Dai, X. 2017, *Monthly Notices of the Royal Astronomical Society*, 468, 49684981, doi: [10.1093/mnras/stx816](https://doi.org/10.1093/mnras/stx816)
- Anderson, J. P., González-Gait3n, S., Hamuy, M., et al. 2014, *The Astrophysical Journal*, 786, 67, doi: [10.1088/0004-637X/786/1/67](https://doi.org/10.1088/0004-637X/786/1/67)
- Anderson, J. P., Contreras, C., Stritzinger, M. D., et al. 2024, *A&A*, 692, A95, doi: [10.1051/0004-6361/202244401](https://doi.org/10.1051/0004-6361/202244401)

- Astropy Collaboration, Robitaille, T. P., Tollerud, E. J., et al. 2013, *A&A*, 558, A33, doi: [10.1051/0004-6361/201322068](https://doi.org/10.1051/0004-6361/201322068)
- Astropy Collaboration, Price-Whelan, A. M., Sipőcz, B. M., et al. 2018, *AJ*, 156, 123, doi: [10.3847/1538-3881/aabc4f](https://doi.org/10.3847/1538-3881/aabc4f)
- Astropy Collaboration, Price-Whelan, A. M., Lim, P. L., et al. 2022, *ApJ*, 935, 167, doi: [10.3847/1538-4357/ac7c74](https://doi.org/10.3847/1538-4357/ac7c74)
- Barbon, R., Ciatti, F., & Rosino, L. 1979, *A&A*, 72, 287
- Barker, B. L., Harris, C. E., Warren, M. L., O' Connor, E. P., & Couch, S. M. 2022, *The Astrophysical Journal*, 934, 67, doi: [10.3847/1538-4357/ac77f3](https://doi.org/10.3847/1538-4357/ac77f3)
- Barker, B. L., O' Connor, E. P., & Couch, S. M. 2023, *The Astrophysical Journal Letters*, 944, L2, doi: [10.3847/2041-8213/acb052](https://doi.org/10.3847/2041-8213/acb052)
- Beasor, E. R., Smith, N., & Jencson, J. E. 2024, *The red supergiant progenitor luminosity problem*, <https://arxiv.org/abs/2410.14027>
- Becker, A. 2015, *HOTPANTS: High Order Transform of PSF ANd Template Subtraction*, *Astrophysics Source Code Library*, record ascl:1504.004
- Bertin, E., & Arnouts, S. 1996, *A&AS*, 117, 393, doi: [10.1051/aas:1996164](https://doi.org/10.1051/aas:1996164)
- Blinnikov, S. I., Eastman, R., Bartunov, O. S., Popolitov, V. A., & Woosley, S. E. 1998, *ApJ*, 496, 454, doi: [10.1086/305375](https://doi.org/10.1086/305375)
- Bloom, J. S., Kulkarni, S. R., & Djorgovski, S. G. 2002, *AJ*, 123, 1111, doi: [10.1086/338893](https://doi.org/10.1086/338893)
- Bostroem, K. A., Valenti, S., Horesh, A., et al. 2019, *Monthly Notices of the Royal Astronomical Society*, 485, 5120, doi: [10.1093/mnras/stz570](https://doi.org/10.1093/mnras/stz570)
- Boutsia, K., Blanc, G., & Beletsky, Y. 2016, *LDSS-3 User Manual*, Las Campanas Observatory. <https://www.lco.cl/technical-documentation/ldss-3-user-manual/>
- Bradley, L., Sipőcz, B., Robitaille, T., et al. 2025, *astropy/photutils: 2.2.0, 2.2.0 Zenodo*, doi: [10.5281/zenodo.596036](https://doi.org/10.5281/zenodo.596036)
- Bruch, R. J., Gal-Yam, A., Schulze, S., et al. 2021, *The Astrophysical Journal*, 912, 46, doi: [10.3847/1538-4357/abef05](https://doi.org/10.3847/1538-4357/abef05)
- Bruch, R. J., Gal-Yam, A., Yaron, O., et al. 2023, *ApJ*, 952, 119, doi: [10.3847/1538-4357/acd8be](https://doi.org/10.3847/1538-4357/acd8be)
- Byler, N., Dalcanton, J. J., Conroy, C., & Johnson, B. D. 2017, *ApJ*, 840, 44, doi: [10.3847/1538-4357/aa6c66](https://doi.org/10.3847/1538-4357/aa6c66)
- Calzetti, D., Armus, L., Bohlin, R. C., et al. 2000, *ApJ*, 533, 682, doi: [10.1086/308692](https://doi.org/10.1086/308692)
- Chambers, K. C., Magnier, E. A., Metcalfe, N., et al. 2016, *arXiv e-prints*, arXiv:1612.05560. <https://arxiv.org/abs/1612.05560>
- Chieffi, A., Domínguez, I., Heflich, P., Limongi, M., & Straniero, O. 2003, *Monthly Notices of the Royal Astronomical Society*, 345, 111, doi: [10.1046/j.1365-8711.2003.06958.x](https://doi.org/10.1046/j.1365-8711.2003.06958.x)
- Chugai, N. N. 2001, *MNRAS*, 326, 1448, doi: [10.1111/j.1365-2966.2001.04717.x](https://doi.org/10.1111/j.1365-2966.2001.04717.x)
- Conroy, C., & Gunn, J. E. 2010, *ApJ*, 712, 833, doi: [10.1088/0004-637X/712/2/833](https://doi.org/10.1088/0004-637X/712/2/833)
- Conroy, C., Gunn, J. E., & White, M. 2009, *ApJ*, 699, 486, doi: [10.1088/0004-637X/699/1/486](https://doi.org/10.1088/0004-637X/699/1/486)
- Coulter, D. A., Jones, D. O., McGill, P., et al. 2022, *YSE-PZ: An Open-source Target and Observation Management System*, v0.3.0 Zenodo, doi: [10.5281/zenodo.7278430](https://doi.org/10.5281/zenodo.7278430)
- Coulter, D. A., Jones, D. O., McGill, P., et al. 2023, *PASP*, 135, 064501, doi: [10.1088/1538-3873/acd662](https://doi.org/10.1088/1538-3873/acd662)
- Dark Energy Survey Collaboration, Abbott, T., Abdalla, F. B., et al. 2016, *MNRAS*, 460, 1270, doi: [10.1093/mnras/stw641](https://doi.org/10.1093/mnras/stw641)
- Davies, B., & Beasor, E. R. 2017, *Monthly Notices of the Royal Astronomical Society*, 474, 2116, doi: [10.1093/mnras/stx2734](https://doi.org/10.1093/mnras/stx2734)
- Davies, B., & Beasor, E. R. 2020, *Monthly Notices of the Royal Astronomical Society*, 493, 468, doi: [10.1093/mnras/staa174](https://doi.org/10.1093/mnras/staa174)
- Davies, B., Plez, B., & Petrault, M. 2022, *Monthly Notices of the Royal Astronomical Society*, 517, 1483, doi: [10.1093/mnras/stac2427](https://doi.org/10.1093/mnras/stac2427)
- de Soto, K. in prep.
- de Soto, K. M., Villar, V. A., Berger, E., et al. 2024, *ApJ*, 974, 169, doi: [10.3847/1538-4357/ad6a4f](https://doi.org/10.3847/1538-4357/ad6a4f)
- de Wit, S., Bonanos, A. Z., Antoniadis, K., et al. 2024, *A&A*, 689, A46, doi: [10.1051/0004-6361/202449607](https://doi.org/10.1051/0004-6361/202449607)
- Dessart, L., & Hillier, D. J. 2005, *A&A*, 439, 671, doi: [10.1051/0004-6361:20053217](https://doi.org/10.1051/0004-6361:20053217)
- Dessart, L., & Hillier, D. J. 2019, *A&A*, 625, A9, doi: [10.1051/0004-6361/201834732](https://doi.org/10.1051/0004-6361/201834732)
- Dessart, L., Hillier, D. J., Waldman, R., & Livne, E. 2013, *Monthly Notices of the Royal Astronomical Society*, 433, 17451763, doi: [10.1093/mnras/stt861](https://doi.org/10.1093/mnras/stt861)
- Dessart, L., Hillier, D. J., Waldman, R., Livne, E., & Yaron, O. 2017, *Astronomy & Astrophysics*, 603, A36, doi: [10.1051/0004-6361/201730942](https://doi.org/10.1051/0004-6361/201730942)
- Dessart, L., & Jacobson-Galán, W. V. 2023, 677, A105, doi: [10.1051/0004-6361/202346754](https://doi.org/10.1051/0004-6361/202346754)
- Dessart, L., Livne, E., & Waldman, R. 2010, *Monthly Notices of the Royal Astronomical Society*, 408, 827840, doi: [10.1111/j.1365-2966.2010.17190.x](https://doi.org/10.1111/j.1365-2966.2010.17190.x)

- Dong, Y., de Soto, K., Villar, V. A., et al. 2025, arXiv e-prints, arXiv:2507.22156, doi: [10.48550/arXiv.2507.22156](https://doi.org/10.48550/arXiv.2507.22156)
- Draine, B. T., & Li, A. 2007, *ApJ*, 657, 810, doi: [10.1086/511055](https://doi.org/10.1086/511055)
- Dyk, S. D. V. 2025, Red Supergiants as Supernova Progenitors, <https://arxiv.org/abs/2507.15973>
- Eastman, R. G., Schmidt, B. P., & Kirshner, R. 1996, *ApJ*, 466, 911, doi: [10.1086/177563](https://doi.org/10.1086/177563)
- Eldridge, J. J., Guo, N. Y., Rodrigues, N., Stanway, E. R., & Xiao, L. 2019, *Publications of the Astronomical Society of Australia*, 36, e041, doi: [10.1017/pasa.2019.31](https://doi.org/10.1017/pasa.2019.31)
- Euclid Collaboration, Mellier, Y., Abdurro'uf, et al. 2025a, *A&A*, 697, A1, doi: [10.1051/0004-6361/202450810](https://doi.org/10.1051/0004-6361/202450810)
- Euclid Collaboration, Romelli, E., Kümmel, M., et al. 2025b, arXiv e-prints, arXiv:2503.15305, doi: [10.48550/arXiv.2503.15305](https://doi.org/10.48550/arXiv.2503.15305)
- Falcón-Barroso, J., Sánchez-Blázquez, P., Vazdekis, A., et al. 2011, *A&A*, 532, A95, doi: [10.1051/0004-6361/201116842](https://doi.org/10.1051/0004-6361/201116842)
- Falk, S. W., & Arnett, W. D. 1977, *ApJS*, 33, 515, doi: [10.1086/190440](https://doi.org/10.1086/190440)
- Fang, Q., Maeda, K., Ye, H., Moriya, T. J., & Matsumoto, T. 2025, *ApJ*, 978, 35, doi: [10.3847/1538-4357/ad8b19](https://doi.org/10.3847/1538-4357/ad8b19)
- Fang, Q., Moriya, T. J., & Maeda, K. 2025a, *The Astrophysical Journal*, 986, 39, doi: [10.3847/1538-4357/adceae](https://doi.org/10.3847/1538-4357/adceae)
- Fang, Q., Moriya, T. J., Maeda, K., Dorozsmai, A., & Silva-Farfán, J. 2025b, arXiv e-prints, arXiv:2507.14665, doi: [10.48550/arXiv.2507.14665](https://doi.org/10.48550/arXiv.2507.14665)
- Fang, Q., Moriya, T. J., Maeda, K., Dorozsmai, A., & Silva-Farfán, J. 2025c, *The Astrophysical Journal*, 990, 60, doi: [10.3847/1538-4357/adf218](https://doi.org/10.3847/1538-4357/adf218)
- Faran, T., Nakar, E., & Poznanski, D. 2017, *Monthly Notices of the Royal Astronomical Society*, 473, 513, doi: [10.1093/mnras/stx2288](https://doi.org/10.1093/mnras/stx2288)
- Ferland, G. J., Porter, R. L., van Hoof, P. A. M., et al. 2013, *RMxAA*, 49, 137. <https://arxiv.org/abs/1302.4485>
- Filippenko, A. V. 1997, *ARA&A*, 35, 309, doi: [10.1146/annurev.astro.35.1.309](https://doi.org/10.1146/annurev.astro.35.1.309)
- Fitzpatrick, E. L., & Massa, D. 2007, *The Astrophysical Journal*, 663, 320341, doi: [10.1086/518158](https://doi.org/10.1086/518158)
- Flaugher, B., Diehl, H. T., Honscheid, K., et al. 2015, *ApJ*, 150, 150, doi: [10.1088/0004-6256/150/5/150](https://doi.org/10.1088/0004-6256/150/5/150)
- Förster, F., Moriya, T. J., Maureira, J. C., et al. 2018, *Nature Astronomy*, 2, 808, doi: [10.1038/s41550-018-0563-4](https://doi.org/10.1038/s41550-018-0563-4)
- Gagliano, A., de Soto, K., Boesky, A., & Manning, T. A. 2025, alexandergagliano/Prost: v1.2.12, v1.2.12 Zenodo, doi: [10.5281/zenodo.15635013](https://doi.org/10.5281/zenodo.15635013)
- Gal-Yam, A. 2012, *Science*, 337, 927, doi: [10.1126/science.1203601](https://doi.org/10.1126/science.1203601)
- Gal-Yam, A. 2017, in *Handbook of Supernovae*, ed. A. W. Alsabti & P. Murdin, 195, doi: [10.1007/978-3-319-21846-5\\_35](https://doi.org/10.1007/978-3-319-21846-5_35)
- Gal-Yam, A., Bruch, R., Schulze, S., et al. 2022, *Nature*, 601, 201204, doi: [10.1038/s41586-021-04155-1](https://doi.org/10.1038/s41586-021-04155-1)
- Galbany, L., Hamuy, M., Phillips, M. M., et al. 2016, *The Astronomical Journal*, 151, 33, doi: [10.3847/0004-6256/151/2/33](https://doi.org/10.3847/0004-6256/151/2/33)
- Gall, E. E. E., Polshaw, J., Kotak, R., et al. 2015, *A&A*, 582, A3, doi: [10.1051/0004-6361/201525868](https://doi.org/10.1051/0004-6361/201525868)
- Gallazzi, A., Charlot, S., Brinchmann, J., White, S. D. M., & Tremonti, C. A. 2005, *MNRAS*, 362, 41, doi: [10.1111/j.1365-2966.2005.09321.x](https://doi.org/10.1111/j.1365-2966.2005.09321.x)
- Géron, T. 2024, DETECT: Detection Efficiency and Threshold Estimation for Characterization of Transients,, GitHub repository <https://github.com/tobiasgeron/detect>
- Ginsburg, A., Sipőcz, B. M., Brasseur, C. E., et al. 2019, *AJ*, 157, 98, doi: [10.3847/1538-3881/aafc33](https://doi.org/10.3847/1538-3881/aafc33)
- Goldberg, J., & Bildsten, L. 2020, *The Astrophysical Journal*, 895, L45, doi: [10.3847/2041-8213/ab9300](https://doi.org/10.3847/2041-8213/ab9300)
- Goldberg, J. A., Bildsten, L., & Paxton, B. 2019, *The Astrophysical Journal*, 879, 3, doi: [10.3847/1538-4357/ab22b6](https://doi.org/10.3847/1538-4357/ab22b6)
- Goldman, S. R., van Loon, J. T., Zijlstra, A. A., et al. 2016, *Monthly Notices of the Royal Astronomical Society*, 465, 403, doi: [10.1093/mnras/stw2708](https://doi.org/10.1093/mnras/stw2708)
- Gonzalez-Gaitan, S., Tominaga, N., Molina, J., et al. 2015, *The Rise-Time of Type II Supernovae*, <https://arxiv.org/abs/1505.02988>
- Graham, M. L., Bellm, E. C., Guy, L. P., et al. 2024, LSST Alerts: Key Numbers (DMTN-102), Tech. Rep. DMTN-102, Vera C. Rubin Observatory Data Management, doi: [10.71929/rubin/2997858](https://doi.org/10.71929/rubin/2997858)
- Grayling, M., Gutiérrez, C. P., Sullivan, M., et al. 2023, *Monthly Notices of the Royal Astronomical Society*, 520, 684701, doi: [10.1093/mnras/stad056](https://doi.org/10.1093/mnras/stad056)
- Gutiérrez, C. P., Anderson, J. P., Hamuy, M., et al. 2017, *The Astrophysical Journal*, 850, 90, doi: [10.3847/1538-4357/aa8f42](https://doi.org/10.3847/1538-4357/aa8f42)
- Hamuy, M. 2003, *ApJ*, 582, 905, doi: [10.1086/344689](https://doi.org/10.1086/344689)
- Healy, S., Horiuchi, S., & Ashall, C. 2024, *The Red Supergiant Problem: As Seen from the Local Group's Red Supergiant Populations*, <https://arxiv.org/abs/2412.04386>
- Hillier, Desmond John, & Dessart, Luc. 2019, *A&A*, 631, A8, doi: [10.1051/0004-6361/201935100](https://doi.org/10.1051/0004-6361/201935100)

- Hinds, K. R., Perley, D. A., Sollerman, J., et al. 2025, *MNRAS*, 541, 135, doi: [10.1093/mnras/staf888](https://doi.org/10.1093/mnras/staf888)
- Hiramatsu, D., Howell, D. A., Moriya, T. J., et al. 2021, *The Astrophysical Journal*, 913, 55, doi: [10.3847/1538-4357/abf6d6](https://doi.org/10.3847/1538-4357/abf6d6)
- Hosseinizadeh, G., Dauphin, F., Villar, V. A., et al. 2020, *The Astrophysical Journal*, 905, 93, doi: [10.3847/1538-4357/abc42b](https://doi.org/10.3847/1538-4357/abc42b)
- Hsu, B., Smith, N., Goldberg, J. A., et al. 2024, arXiv e-prints, arXiv:2408.07874, doi: [10.48550/arXiv.2408.07874](https://doi.org/10.48550/arXiv.2408.07874)
- Irani, I., Morag, J., Gal-Yam, A., et al. 2024, *ApJ*, 970, 96, doi: [10.3847/1538-4357/ad3de8](https://doi.org/10.3847/1538-4357/ad3de8)
- Jacobson-Galán, W. V., Dessart, L., Jones, D. O., et al. 2022, *The Astrophysical Journal*, 924, 15, doi: [10.3847/1538-4357/ac3f3a](https://doi.org/10.3847/1538-4357/ac3f3a)
- Jacobson-Galán, W. V., Dessart, L., Jones, D. O., et al. 2022, *ApJ*, 924, 15, doi: [10.3847/1538-4357/ac3f3a](https://doi.org/10.3847/1538-4357/ac3f3a)
- Jacobson-Galán, W. V., Dessart, L., Davis, K. W., et al. 2024, *The Astrophysical Journal*, 970, 189, doi: [10.3847/1538-4357/ad4a2a](https://doi.org/10.3847/1538-4357/ad4a2a)
- Jerkstrand, A., Milisavljevic, D., & Müller, B. 2025, *Core-collapse supernovae*, <https://arxiv.org/abs/2503.01321>
- Johnson, B. D., Leja, J., Conroy, C., & Speagle, J. S. 2021, *ApJS*, 254, 22, doi: [10.3847/1538-4365/abef67](https://doi.org/10.3847/1538-4365/abef67)
- Jones, D. O., Foley, R. J., Narayan, G., et al. 2021, *ApJ*, 908, 143, doi: [10.3847/1538-4357/abd7f5](https://doi.org/10.3847/1538-4357/abd7f5)
- Jones, D. O., McGill, P., Manning, T. A., et al. 2024, arXiv e-prints, arXiv:2410.17322, doi: [10.48550/arXiv.2410.17322](https://doi.org/10.48550/arXiv.2410.17322)
- Kasen, D., & Woosley, S. E. 2009, *ApJ*, 703, 2205, doi: [10.1088/0004-637X/703/2/2205](https://doi.org/10.1088/0004-637X/703/2/2205)
- Kelly, P. L., & Kirshner, R. P. 2012, *The Astrophysical Journal*, 759, 107, doi: [10.1088/0004-637x/759/2/107](https://doi.org/10.1088/0004-637x/759/2/107)
- Kessler, R., Narayan, G., Avelino, A., et al. 2019, *Publications of the Astronomical Society of the Pacific*, 131, 094501, doi: [10.1088/1538-3873/ab26f1](https://doi.org/10.1088/1538-3873/ab26f1)
- Khatami, D., & Kasen, D. 2024, *The Landscape of Thermal Transients from Supernova Interacting with a Circumstellar Medium*, <https://arxiv.org/abs/2304.03360>
- Khazov, D., Yaron, O., Gal-Yam, A., et al. 2016, *The Astrophysical Journal*, 818, 3, doi: [10.3847/0004-637X/818/1/3](https://doi.org/10.3847/0004-637X/818/1/3)
- Kilpatrick, C. D., Izzo, L., Bentley, R. O., et al. 2023, *Monthly Notices of the Royal Astronomical Society*, 524, 21612185, doi: [10.1093/mnras/stad1954](https://doi.org/10.1093/mnras/stad1954)
- Kirshner, R. P., & Kwan, J. 1974, *ApJ*, 193, 27, doi: [10.1086/153123](https://doi.org/10.1086/153123)
- Kochanek, C. S. 2018, *Monthly Notices of the Royal Astronomical Society*, 483, 3762, doi: [10.1093/mnras/sty3363](https://doi.org/10.1093/mnras/sty3363)
- Kochanek, C. S. 2020, *Monthly Notices of the Royal Astronomical Society*, 493, 49454949, doi: [10.1093/mnras/staa605](https://doi.org/10.1093/mnras/staa605)
- Kochanek, C. S., Beacom, J. F., Kistler, M. D., et al. 2008, *The Astrophysical Journal*, 684, 13361342, doi: [10.1086/590053](https://doi.org/10.1086/590053)
- Kozyreva, A., Klencki, J., Filippenko, A. V., et al. 2022, *The Astrophysical Journal Letters*, 934, L31, doi: [10.3847/2041-8213/ac835a](https://doi.org/10.3847/2041-8213/ac835a)
- Kriek, M., & Conroy, C. 2013, *ApJL*, 775, L16, doi: [10.1088/2041-8205/775/1/L16](https://doi.org/10.1088/2041-8205/775/1/L16)
- Kroupa, P., & Jerabkova, T. 2021, arXiv e-prints, arXiv:2112.10788, doi: [10.48550/arXiv.2112.10788](https://doi.org/10.48550/arXiv.2112.10788)
- Kümmel, M., Álvarez-Ayllón, A., Bertin, E., et al. 2022, arXiv e-prints, arXiv:2212.02428, doi: [10.48550/arXiv.2212.02428](https://doi.org/10.48550/arXiv.2212.02428)
- Leja, J., Johnson, B. D., Conroy, C., et al. 2019, *ApJ*, 877, 140, doi: [10.3847/1538-4357/ab1d5a](https://doi.org/10.3847/1538-4357/ab1d5a)
- Leja, J., Speagle, J. S., Ting, Y.-S., et al. 2022, *The Astrophysical Journal*, 936, 165, doi: [10.3847/1538-4357/ac887d](https://doi.org/10.3847/1538-4357/ac887d)
- Levesque, E. M., Massey, P., Olsen, K. A. G., et al. 2005, *The Astrophysical Journal*, 628, 973, doi: [10.1086/430901](https://doi.org/10.1086/430901)
- Li, W., Leaman, J., Chornock, R., et al. 2011, *MNRAS*, 412, 1441, doi: [10.1111/j.1365-2966.2011.18160.x](https://doi.org/10.1111/j.1365-2966.2011.18160.x)
- LSST Science Collaboration, Abell, P. A., Allison, J., et al. 2009, *LSST Science Book, Version 2.0*, <https://arxiv.org/abs/0912.0201>
- Martinez, L., Anderson, J. P., Bersten, M. C., et al. 2022a, *Astronomy & Astrophysics*, 660, A42, doi: [10.1051/0004-6361/202142555](https://doi.org/10.1051/0004-6361/202142555)
- Martinez, L., Bersten, M. C., Anderson, J. P., et al. 2022b, *Astronomy & Astrophysics*, 660, A40, doi: [10.1051/0004-6361/202142075](https://doi.org/10.1051/0004-6361/202142075)
- Martinez, L., Bersten, M. C., Anderson, J. P., et al. 2022c, *Astronomy & Astrophysics*, 660, A41, doi: [10.1051/0004-6361/202142076](https://doi.org/10.1051/0004-6361/202142076)
- Masci, F. J., Laher, R. R., Rusholme, B., et al. 2018, *Publications of the Astronomical Society of the Pacific*, 131, 018003, doi: [10.1088/1538-3873/aae8ac](https://doi.org/10.1088/1538-3873/aae8ac)
- Matsumoto, T., & Metzger, B. D. 2022, *The Astrophysical Journal*, 936, 114, doi: [10.3847/1538-4357/ac892c](https://doi.org/10.3847/1538-4357/ac892c)
- Miller, A. A., Abrams, N. S., Aldering, G., et al. 2025, arXiv e-prints, arXiv:2503.14579, doi: [10.48550/arXiv.2503.14579](https://doi.org/10.48550/arXiv.2503.14579)

- Moriya, T. J., Förster, F., Yoon, S.-C., Gräfenner, G., & Blinnikov, S. I. 2018, *Monthly Notices of the Royal Astronomical Society*, 476, 2840, doi: [10.1093/mnras/sty475](https://doi.org/10.1093/mnras/sty475)
- Moriya, T. J., Subrayan, B. M., Milisavljevic, D., & Blinnikov, S. I. 2023, *Publications of the Astronomical Society of Japan*, 75, 634, doi: [10.1093/pasj/psad024](https://doi.org/10.1093/pasj/psad024)
- Morozova, V., Piro, A. L., & Valenti, S. 2017, *The Astrophysical Journal*, 838, 28, doi: [10.3847/1538-4357/aa6251](https://doi.org/10.3847/1538-4357/aa6251)
- Morozova, V., Piro, A. L., & Valenti, S. 2018, *The Astrophysical Journal*, 858, 15, doi: [10.3847/1538-4357/aab9a6](https://doi.org/10.3847/1538-4357/aab9a6)
- Müller, T., Prieto, J. L., Pejcha, O., & Clocchiatti, A. 2017, *ApJ*, 841, 127, doi: [10.3847/1538-4357/aa72f1](https://doi.org/10.3847/1538-4357/aa72f1)
- Murphey, C. T., Nair, G., Narayan, G., et al. 2025, *Transient Name Server Discovery Report*, 2025-975, 1
- Murphey, T. in prep.
- Nagao, T., Reynolds, T., Kuncarayakti, H., et al. 2025, *Astronomy & Astrophysics*, 699, doi: [10.1051/0004-6361/202554988](https://doi.org/10.1051/0004-6361/202554988)
- Nagy, A. P., & Vinkó, J. 2016, *Astronomy & Astrophysics*, 589, A53, doi: [10.1051/0004-6361/201527931](https://doi.org/10.1051/0004-6361/201527931)
- Neustadt, J. M. M., Kochanek, C. S., Stanek, K. Z., et al. 2021, *Monthly Notices of the Royal Astronomical Society*, 508, 516528, doi: [10.1093/mnras/stab2605](https://doi.org/10.1093/mnras/stab2605)
- NSF-DOE Vera C. Rubin Observatory. 2025, *Legacy Survey of Space and Time Data Preview 1 [Data set]*, NSF-DOE Vera C. Rubin Observatory, doi: [10.71929/RUBIN/2570308](https://doi.org/10.71929/RUBIN/2570308)
- Nugent, A. E., Villar, V. A., Gagliano, A., et al. 2025, *arXiv e-prints*, arXiv:2509.08874, doi: [10.48550/arXiv.2509.08874](https://doi.org/10.48550/arXiv.2509.08874)
- Patat, F., Barbon, R., Cappellaro, E., & Turatto, M. 1994, *A&A*, 282, 731
- Paxton, B., Schwab, J., Bauer, E. B., et al. 2018, *ApJS*, 234, 34, doi: [10.3847/1538-4365/aaa5a8](https://doi.org/10.3847/1538-4365/aaa5a8)
- Pejcha, O., & Prieto, J. L. 2015, *The Astrophysical Journal*, 806, 225, doi: [10.1088/0004-637x/806/2/225](https://doi.org/10.1088/0004-637x/806/2/225)
- Perley, D. A., Fremling, C., Sollerman, J., et al. 2020, *The Astrophysical Journal*, 904, 35, doi: [10.3847/1538-4357/abbd98](https://doi.org/10.3847/1538-4357/abbd98)
- Pessi, P. J., Anderson, J. P., Folatelli, G., et al. 2023, *MNRAS*, 523, 5315, doi: [10.1093/mnras/stad1822](https://doi.org/10.1093/mnras/stad1822)
- Planck Collaboration, Ade, P. A. R., Aghanim, N., et al. 2016, *A&A*, 594, A13, doi: [10.1051/0004-6361/201525830](https://doi.org/10.1051/0004-6361/201525830)
- Popesso, P., Concas, A., Cresci, G., et al. 2022, *Monthly Notices of the Royal Astronomical Society*, 519, 15261544, doi: [10.1093/mnras/stac3214](https://doi.org/10.1093/mnras/stac3214)
- Popov, D. V. 1993, *ApJ*, 414, 712, doi: [10.1086/173117](https://doi.org/10.1086/173117)
- Ransome, C. L., & Villar, V. A. 2025, *The Astrophysical Journal*, 987, 13, doi: [10.3847/1538-4357/adce03](https://doi.org/10.3847/1538-4357/adce03)
- Rest, A., & SuperMACHO. 2004, in *American Astronomical Society Meeting Abstracts*, Vol. 205, American Astronomical Society Meeting Abstracts, 28.02
- Rest, A., Scolnic, D., Foley, R. J., et al. 2014, *ApJ*, 795, 44, doi: [10.1088/0004-637X/795/1/44](https://doi.org/10.1088/0004-637X/795/1/44)
- Rose, B. M., Baltay, C., Hounsell, R., et al. 2021, *A Reference Survey for Supernova Cosmology with the Nancy Grace Roman Space Telescope*, <https://arxiv.org/abs/2111.03081>
- Rubin Observatory Project. 2025, *An Interim Report on the ComCam OnSky Campaign (SITCOMTN149)*, <https://sitcomtn-149.lsst.io/>, <https://sitcomtn-149.lsst.io/>
- Rubin Observatory Science Pipelines Developers. 2025, *The LSST Science Pipelines Software: Optical Survey Pipeline Reduction and Analysis Environment*, Project Science Technical Note PSTN-019, NSF-DOE Vera C. Rubin Observatory, doi: [10.71929/rubin/2570545](https://doi.org/10.71929/rubin/2570545)
- Sanders, N. E., Soderberg, A. M., Gezari, S., et al. 2015, *The Astrophysical Journal*, 799, 208, doi: [10.1088/0004-637X/799/2/208](https://doi.org/10.1088/0004-637X/799/2/208)
- Schechter, P. L., Mateo, M., & Saha, A. 1993, *PASP*, 105, 1342, doi: [10.1086/133316](https://doi.org/10.1086/133316)
- Schlafly, E. F., & Finkbeiner, D. P. 2011a, *ApJ*, 737, 103, doi: [10.1088/0004-637X/737/2/103](https://doi.org/10.1088/0004-637X/737/2/103)
- Schlafly, E. F., & Finkbeiner, D. P. 2011b, *ApJ*, 737, 103, doi: [10.1088/0004-637X/737/2/103](https://doi.org/10.1088/0004-637X/737/2/103)
- Schlegel, D. J., Finkbeiner, D. P., & Davis, M. 1998, *ApJ*, 500, 525, doi: [10.1086/305772](https://doi.org/10.1086/305772)
- Schulze, S., Yaron, O., Sollerman, J., et al. 2021, *The Astrophysical Journal Supplement Series*, 255, 29, doi: [10.3847/1538-4365/abff5e](https://doi.org/10.3847/1538-4365/abff5e)
- Shussman, T., Waldman, R., & Nakar, E. 2016, *Type II supernovae Early Light Curves*, <https://arxiv.org/abs/1610.05323>
- Silva-Farfán, J., Förster, F., Moriya, T. J., et al. 2024, *The Astrophysical Journal*, 969, 57, doi: [10.3847/1538-4357/ad402a](https://doi.org/10.3847/1538-4357/ad402a)
- Skrutskie, M. F., Cutri, R. M., Stiening, R., et al. 2006, *AJ*, 131, 1163, doi: [10.1086/498708](https://doi.org/10.1086/498708)
- Smartt, S. J. 2015, *PASA*, 32, e016, doi: [10.1017/pasa.2015.17](https://doi.org/10.1017/pasa.2015.17)
- Smartt, S. J., Eldridge, J. J., Crockett, R. M., & Maund, J. R. 2009, *MNRAS*, 395, 1409, doi: [10.1111/j.1365-2966.2009.14506.x](https://doi.org/10.1111/j.1365-2966.2009.14506.x)
- Smith, N., Li, W., Filippenko, A. V., & Chornock, R. 2011, *MNRAS*, 412, 1522, doi: [10.1111/j.1365-2966.2011.17229.x](https://doi.org/10.1111/j.1365-2966.2011.17229.x)

- Speagle, J. S. 2020, MNRAS, doi: [10.1093/mnras/staa278](https://doi.org/10.1093/mnras/staa278)
- Strotjohann, N. L., Ofek, E. O., & Gal-Yam, A. 2024, A bias-corrected luminosity function for red supergiant supernova progenitor stars, <https://arxiv.org/abs/2311.00744>
- Sukhbold, T., Ertl, T., Woosley, S. E., Brown, J. M., & Janka, H. T. 2016, ApJ, 821, 38, doi: [10.3847/0004-637X/821/1/38](https://doi.org/10.3847/0004-637X/821/1/38)
- Thornton, I., Villar, V. A., Gomez, S., & Hosseinzadeh, G. 2024, Research Notes of the American Astronomical Society, 8, 48, doi: [10.3847/2515-5172/ad28ba](https://doi.org/10.3847/2515-5172/ad28ba)
- Tominaga, N., Morokuma, T., Blinnikov, S. I., et al. 2011, The Astrophysical Journal Supplement Series, 193, 20, doi: [10.1088/0067-0049/193/1/20](https://doi.org/10.1088/0067-0049/193/1/20)
- Tonry, J. L., Denneau, L., Heinze, A. N., et al. 2018, PASP, 130, 064505, doi: [10.1088/1538-3873/aabadf](https://doi.org/10.1088/1538-3873/aabadf)
- Tyson, J. 2002, SPIE Proceedings, doi: [10.1117/12.456772](https://doi.org/10.1117/12.456772)
- Valenti, S., Howell, D. A., Stritzinger, M. D., et al. 2016, MNRAS, 459, 3939, doi: [10.1093/mnras/stw870](https://doi.org/10.1093/mnras/stw870)
- van Loon, J. T., Zijlstra, A. A., Bujarrabal, V., & Nyman, L.-Å. 2001, A&A, 368, 950, doi: [10.1051/0004-6361:20010052](https://doi.org/10.1051/0004-6361:20010052)
- Villar, V. A., Berger, E., Miller, G., et al. 2019, The Astrophysical Journal, 884, 83, doi: [10.3847/1538-4357/ab418c](https://doi.org/10.3847/1538-4357/ab418c)
- Walmswell, J. J., & Eldridge, J. J. 2012, Monthly Notices of the Royal Astronomical Society, 419, 2054, doi: [10.1111/j.1365-2966.2011.19860.x](https://doi.org/10.1111/j.1365-2966.2011.19860.x)
- Waxman, E., & Katz, B. 2017, Shock Breakout Theory (Springer International Publishing), 9671015, doi: [10.1007/978-3-319-21846-5\\_33](https://doi.org/10.1007/978-3-319-21846-5_33)
- Wright, E. L., Eisenhardt, P. R. M., Mainzer, A. K., et al. 2010, AJ, 140, 1868, doi: [10.1088/0004-6256/140/6/1868](https://doi.org/10.1088/0004-6256/140/6/1868)
- Yaron, O., Perley, D. A., Gal-Yam, A., et al. 2017, Nature Physics, 13, 510, doi: [10.1038/nphys4025](https://doi.org/10.1038/nphys4025)
- Young, T. R. 2004, The Astrophysical Journal, 617, 1233, doi: [10.1086/425675](https://doi.org/10.1086/425675)